

Coordinated Multi-Robot Trajectory Tracking Control over Sampled Communication [★]

Enrica Rossi ^a, Marco Tognon ^b, Luca Ballotta ^a, Ruggero Carli ^a, Juan Cortés ^c,
Antonio Franchi ^{c,d}, Luca Schenato ^a

^a*Department of Information Engineering, University of Padova, Italy*

^b*Autonomous Systems Lab, Department of Mechanical and Process Engineering, ETH Zurich, 8092 Zürich, Switzerland*

^c*LAAS-CNRS, Université de Toulouse, CNRS, Toulouse, France*

^d*Robotics and Mechatronics lab, University of Twente, Enschede, The Netherlands*

Abstract

In this paper, we propose an inverse-kinematics controller for a class of multi-robot systems in the scenario of sampled communication. The goal is to make a group of robots perform trajectory tracking in a coordinated way when the sampling time of communications is much larger than the sampling time of low-level controllers, disrupting theoretical convergence guarantees of standard control design in continuous time. Given a desired trajectory in configuration space which is pre-computed offline, the proposed controller receives configuration measurements, possibly via wireless, to re-compute velocity references for the robots, which are tracked by a low-level controller. We propose [joint design of a sampled proportional feedback plus a novel continuous-time feedforward that linearizes the dynamics around the reference trajectory: this method](#) is amenable to distributed communication implementation where only one broadcast transmission is needed per sample. Also, we provide closed-form expressions for instability and stability regions and convergence rate in terms of proportional gain k and sampling period T . We test the proposed control strategy via numerical simulations in the scenario of cooperative aerial manipulation of a cable-suspended load using a realistic simulator (*Fly-Crane*). Finally, we compare our proposed controller with centralized approaches that adapt the feedback gain online through smart heuristics, and show that it achieves comparable performance.

Key words: Control over sampled communications; distributed control; multi-robot systems; trajectory tracking; UAVs.

1 Introduction

Unmanned Aerial Vehicles (UAVs) are used in the context of mobile robotics to perform surveillance, coverage, exploration, and transportation [18]. Generally speaking, a group of robots allows to improve task performance with respect to (w.r.t.) the single-robot solution.

[★] This work Partially funded by: the European Commission project H2020 AERIAL-CORE (EC 871479), the ANR, Project ANR-17-CE33-0007 MuRoPhen and by University of Padova grant “Magic” SCHE_SID17_01.

Email addresses: enrica.rossi.1@studenti.unipd.it (Enrica Rossi), mtognon@ethz.ch (Marco Tognon), ballotta@dei.unipd.it (Luca Ballotta), carlirug@dei.unipd.it (Ruggero Carli), juan.cortes@laas.fr (Juan Cortés), antonio.franchi@laas.fr, a.franchi@utwente.nl (Antonio Franchi), schenato@dei.unipd.it (Luca Schenato).

The use of multiple robots can mitigate problems as the limited payload and time of flight [2]. However, they require careful consideration of cooperation or coordination strategies to achieve common goals [6]. Consider a group of UAVs that transports a load while avoiding obstacles or passing through narrow apertures. In this case, not only each UAV has to avoid obstacles, but also the overall multi-robot system should move in a coordinated way such that the load avoids obstacles, as well [4].

One of the most direct approaches to control multi-robot systems is the centralized kinematic/dynamic inversion [1, 16, 17, 26, 31]. Because of its nature, failure of the central unit may cause the whole task to fail. Distributed and decentralized approaches spread computations across the robots, guaranteeing greater robustness and flexibility w.r.t. a centralized one [25]. Although such approaches are preferable for multi-robot systems, they often lack global information such as load state and

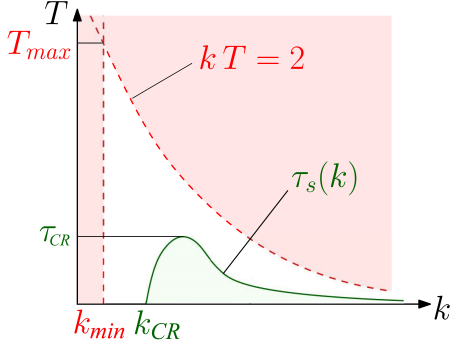


Fig. 1. We propose a controller for trajectory tracking when measurements are transmitted every T seconds, with feedback proportional gain k . We show that, if (k, T) lies outside the dashed red curve, the tracking error is not ρ -monotonically contractive, while zero tracking error is guaranteed if (k, T) lies below the solid green curve $\tau_s(k)$. In particular, there exist sampling time T_{max} such that no gain k can guarantee convergence if $T > T_{max}$ and sampling time τ_{CR} such that a stabilizing gain exists for any $T < \tau_{CR}$.

parameters, or the total number of robots. This aspect increases the difficulty of the controller design and might even degrade performance. Examples of distributed control methods, where robots explicitly exchange local data, can be found for groups of ground [5, 10, 20, 22], underwater [3, 30], and aerial robots [19]. Conversely, decentralized control strategies allow for no direct communication among robots, with examples including ground or aerial manipulators [29, 36]. Also, to reduce communication issues, communication-less approaches relying on a leader-follower paradigm were presented for cooperative transportation and manipulation [7, 11, 33, 35, 37]. In these cases, communication is implicitly given by forces exerted on the load [34]. However, force feedback may be insufficient for precise tracking, because it lacks pose information. The latter can be retrieved by communication among robots, e.g., making them exchange poses, or installing a sensor on the load to broadcast its pose. This setup can also be extended to formation control problems where a group of robots needs to complete a task [8, 9]. For example, a common goal is mapping or surveillance of an area while robots keep a certain 3D formation in order to, e.g., minimize overlaps among their fields of view [27]. In this case, communication-based approaches let robots exchange group-level measurements, such as relative distances.

In applications, limited bandwidth of wireless channels disrupts the assumption of continuous-measurement feedback. As so, specific strategies are needed to deal with sampled communication [12, 15, 32]. However, little work is currently available for multi-robot manipulation.

1.1 Preview of Key Results

In this paper, we aim to design a multi-robot distributed communication controller for trajectory tracking when

wireless communication induces non-negligible sampling of feedback measurements. In this context, a distributed implementation is preferred because (i) it reduces the overall communication burden and related issues such as packet loss or latency, and (ii) it enhances system robustness and scalability. Inspired by previous work [24] where point-stabilization was considered, here we propose a novel *Sampled communication-aware Inverse-Kinematic controller for Multi-robot systems* (SIKM) to address the challenging problem of trajectory tracking under sampled communication. Our contributions are summarized as follows.

- We develop a distributed SIKM controller for trajectory tracking that receives sampled measurements and re-computes reference robot velocities along the trajectory, exploiting a novel continuous-time feedforward term that allows exact trajectory tracking even in the presence of sampled communication.
- We show that, differently from [24], there are a maximum sampling time T_{max} and a minimum feedback gain k_{min} beyond which trajectory tracking cannot be achieved, as graphically depicted in red in Fig. 1.
- We provide closed-form expressions, whose coefficients can be numerically computed, for the stability region (graphically depicted in green in Fig. 1) and for the (exponential) convergence rate of the trajectory tracking error norm in terms of communication sampling period T and feedback gain k . Specifically, we consider stability in terms of ρ -monotonic contractiveness, which, roughly speaking, ensures that the actual trajectory monotonically decreases the tracking error overtime in the absence of external disturbances and is bounded away from singular points.
- We validated our strategy by testing the controller on a realistic dynamical simulator which replicates with high accuracy the experimental setup available at LAAS-CNRS Lab, *Fly-Crane* [26], including dynamical inertial terms, motor actuators, sensor noise, and real-time embedded software implementation.

1.2 Paper Outline

In Section 2 we introduce the class of considered multi-robot systems, provide the kinematic model (Section 2.1), and give an example of real system (Section 2.2). In Section 3 we review control architectures for trajectory tracking, and present our proposed SIKM controller in Section 3.1. In Section 4 we derive fundamental stability limitations in terms of feedback gain and sampling time. In Section 5 we compute an upper bound for the convergence rate, outline a numerical procedure to estimate it from data (Section 5.1), and explicitly find controller parameters that yield the fastest convergence (Section 5.2). In Section 6 we test our controller on a realistic simulator of the *Fly-Crane*, showing that it outperforms standard designs under sampled communication. Final remarks are drawn in Section 7.

2 System Model and Problem Formulation

2.1 Kinematics of Multi-Robot Systems

In this section, we describe the kinematic model of a multi-robot system composed of N robots that exchange state information with a common *pivot*, labeled as V , to fulfill a task. As so, robots need not communicate among themselves, but they implicitly coordinate their motions by communicating with the pivot. The pivot may be an object to be manipulated, a robot to be escorted, or a vehicle in the space. The kinematic model is given by

$$[\mathbf{p}_1 \ \dots \ \mathbf{p}_N]^\top = \mathbf{h}(\mathbf{q}) = [\mathbf{h}^{(1)}(\mathbf{q}_1, \mathbf{q}_V) \ \dots \ \mathbf{h}^{(N)}(\mathbf{q}_N, \mathbf{q}_V)]^\top.$$

This function maps the Lagrangian coordinates of the system $\mathbf{q} = [\mathbf{q}_1^\top \ \dots \ \mathbf{q}_N^\top \ \mathbf{q}_V^\top]^\top \in \mathbb{R}^m$ to the vector collecting the robots configurations $\mathbf{p} = [\mathbf{p}_1^\top \ \dots \ \mathbf{p}_N^\top]^\top \in \mathbb{R}^n$. In particular, $\mathbf{p}_i \in \mathbb{R}^{n_i}$ is the position of the i th robot in space, $\mathbf{q}_i \in \mathbb{R}^{m_i}$ gathers the angles and/or distances between the pivot V and the i th robot, and $\mathbf{q}_V \in \mathbb{R}^{m_V}$ represents the pose (position and orientation) of the pivot. Notice that $m = \sum_{i=1}^N m_i + m_V$ and $n = \sum_{i=1}^N n_i$. The differential kinematics of the system is

$$\dot{\mathbf{p}} = \mathbf{A}_q \dot{\mathbf{q}}, \quad (1)$$

where the Jacobian $\mathbf{A}_q = \frac{\partial \mathbf{h}(\mathbf{q})}{\partial \mathbf{q}} \in \mathbb{R}^{n \times m}$ has structure

$$\mathbf{A}_q = \begin{bmatrix} \mathbf{A}_{q_1}^{(1)} & \mathbf{0} & \mathbf{A}_{q_V}^{(1)} \\ & \ddots & \vdots \\ \mathbf{0} & \mathbf{A}_{q_N}^{(N)} & \mathbf{A}_{q_V}^{(N)} \end{bmatrix}, \quad (2)$$

$\mathbf{A}_{q_i}^{(i)} = \frac{\partial \mathbf{h}^{(i)}(\mathbf{q}_i, \mathbf{q}_V)}{\partial \mathbf{q}_i} \in \mathbb{R}^{n_i \times m_i}$ and $\mathbf{A}_{q_V}^{(i)} = \frac{\partial \mathbf{h}^{(i)}(\mathbf{q}_i, \mathbf{q}_V)}{\partial \mathbf{q}_V} \in \mathbb{R}^{n_i \times m_V}$. We focus on the case $n = m$, corresponding to *square systems*. Let us make an example to justify this choice. Consider the multi-robot system in Fig. 2a, where robots are linked to a platform through rigid cables, and assume that \mathbf{A}_q is invertible and that desired robot velocities $\dot{\mathbf{p}}^d$ are assigned *a priori*. In this case, there always exists a vector $\dot{\mathbf{q}} = \mathbf{A}_q^{-1} \dot{\mathbf{p}}^d$ in configuration space that allows the robots to achieve the desired velocity. The next section expands this example more in details. If $n \neq m$, the Jacobian is not square. In particular, the system is redundant if $n > m$. If $n < m$, there exist trajectories $\dot{\mathbf{q}}$ in the configuration space which are infeasible for any input $\dot{\mathbf{p}}^d$. Such cases require a dedicated analysis which goes beyond the scope of this paper. We refer to the preprint [23] for such an analysis, that, with some attention, allows to integrate the control strategy studied here into more general systems.

Furthermore, we consider a cascade control architecture where we design the proposed SIKM controller at the kinematic level. The latter provides the desired motor

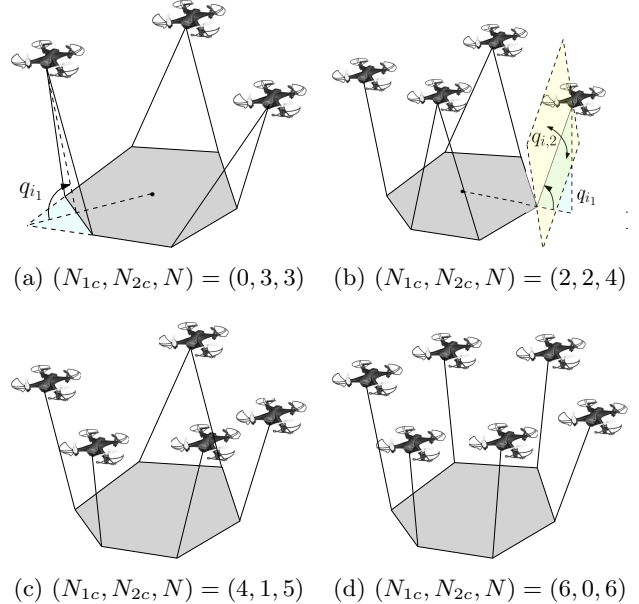


Fig. 2. Square systems where a common object is manipulated by a group of UAVs. All the possible combinations of (N_{1c}, N_{2c}, N) introduced in Sec. 2.2 are represented.

velocities which are tracked by low-level dynamics controllers (see Fig. 4), assuming that these have larger closed-loop bandwidth than the SIKM. This assumption is indeed validated by extensive simulations of the proposed architecture on a full dynamical model (including low-level dynamics as well as external disturbances) with a realistic simulator of the testbed *Fly-Crane*.

2.2 Examples of Square Systems

In the literature, we can find several examples of square systems. One is the multi-robot system depicted in Fig. 2a (called *Fly-Crane* [16]), where three UAVs transport a common platform. Each robot is linked to the load through two rigid cables. The generalized coordinates are chosen as $\mathbf{q} = [q_1 \ q_2 \ q_3 \ \mathbf{q}_V^\top]^\top$. The robot positions $\mathbf{p}_i \in \mathbb{R}^3$ are collected in the vector $\mathbf{p} = [\mathbf{p}_1^\top \ \mathbf{p}_2^\top \ \mathbf{p}_3^\top]^\top$. Thus, the velocity vectors $\dot{\mathbf{q}}, \dot{\mathbf{p}} \in \mathbb{R}^9$ have the same dimension and $\mathbf{A}_q \in \mathbb{R}^{9 \times 9}$ is a square matrix. However, this is a particular case of a larger class: different square systems can be obtained by simply changing the number of robots transporting the platform or the number of cables linking each robot to it. Notice that if one cable was used instead of two, as shown in Fig. 2b, then $\mathbf{q}_i = [q_{i1} \ q_{i2}]^\top \in \mathbb{R}^2$ because each cable can move in two directions (assuming that movements about the cable axis are not allowed). In this case, the system is no more guaranteed to be square. In particular, it holds $n = 3N$ and $m = 6 + 2N_{1c} + N_{2c}$ where $N_{1c} \geq 0$ is the number of robots linked to the load through one cable and $N_{2c} \geq 0$ indicates the number of robots linked through two cables. We have that $N = N_{1c} + N_{2c}$ and, for a square system $n = m$, it must be $3N = 6 + 2N_{1c} + N_{2c}$.

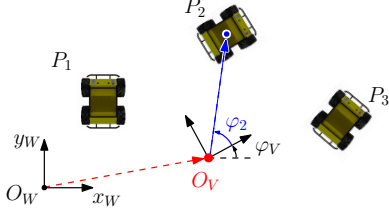


Fig. 3. Representation of a multi-robot system where three robots must keep the same orientation φ_i w.r.t. the reference frame centered in the point O_c during the assigned task.

From these relations it turns out that $N_{2c} \leq 3$, $N_{1c} \leq 6$ and $N \leq 6$; in particular, the possible configurations (N_{1c}, N_{2c}, N) are: (0,3,3) in Fig. 2a, (2,2,4) in Fig. 2b, (4,1,5) in Fig. 2c, (6,0,6) in Fig. 2d.

Other examples of square systems are found in the context of formation control problems [9], as the one represented in Fig. 3. Three ground robots move in a 2-dimensional space while respecting some constraints w.r.t. the frame $\mathcal{F}_V = \{O_V, \mathbf{x}_V, \mathbf{y}_V\}$ representing the pivot (e.g., the barycenter of the system). The position P_i of each robot, defined by the vector $\mathbf{p}_i = [x_i \ y_i]^\top$, is described as a function of: the pivot position $\mathbf{p}_V = [x_V \ y_V]^\top$, the distance d_i from P_i to O_V , the angle φ_i between the line $O_V - P_i$ and the axis \mathbf{x}_V , and the angle φ_V between \mathbf{x}_V and \mathbf{x}_W of the world reference frame $\mathcal{F}_W = \{O_W, \mathbf{x}_W, \mathbf{y}_W\}$. It is trivial to express the position P_i w.r.t. \mathcal{F}_W :

$$\mathbf{p}_i = \mathbf{h}(\mathbf{q}_i, \mathbf{q}_V),$$

where $\mathbf{q}_i = [d_i \ \varphi_i]^\top \in \mathbb{R}^2$, $\mathbf{q}_V = [x_V \ y_V \ \varphi_V]^\top \in \mathbb{R}^3$ and

$$\mathbf{h}(\mathbf{q}_i, \mathbf{q}_V) = \begin{bmatrix} x_V \\ y_V \end{bmatrix} + \begin{bmatrix} \cos(\varphi_V) & -\sin(\varphi_V) \\ \sin(\varphi_V) & \cos(\varphi_V) \end{bmatrix} \begin{bmatrix} d_i \cos(\varphi_i) \\ d_i \sin(\varphi_i) \end{bmatrix}.$$

Let us define the vector of robot positions as $\mathbf{p} = [\mathbf{p}_1^\top \ \mathbf{p}_2^\top \ \mathbf{p}_3^\top]^\top \in \mathbb{R}^6$ and the vector of generalized coordinates as $\mathbf{q} = [\mathbf{q}_1^\top \ \mathbf{q}_2^\top \ \mathbf{q}_3^\top \ \mathbf{q}_V^\top]^\top \in \mathbb{R}^9$. Hence, we can write $\mathbf{h}(\mathbf{q}) \stackrel{\text{def}}{=} [\mathbf{h}(\mathbf{q}_1, \mathbf{q}_V)^\top \ \mathbf{h}(\mathbf{q}_2, \mathbf{q}_V)^\top \ \mathbf{h}(\mathbf{q}_3, \mathbf{q}_V)^\top]^\top$. We assume that the robots must perform a task while keeping the angles φ_i constant w.r.t. \mathcal{F}_V , hence the differential kinematic model is:

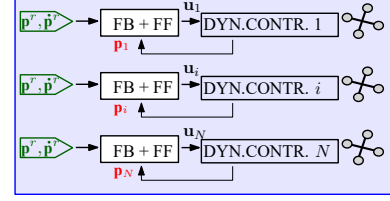
$$\dot{\mathbf{p}} = \mathbf{A}_q \dot{\mathbf{q}}',$$

where $\dot{\mathbf{q}}' = [\dot{q}_V^\top \ \dot{d}_1 \ \dot{d}_2 \ \dot{d}_3]^\top$ and

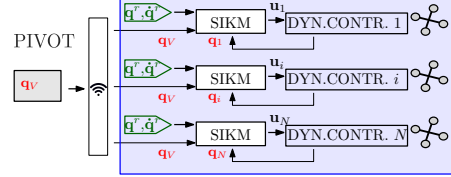
$$\mathbf{A}_q = \begin{bmatrix} \frac{\partial \mathbf{h}(\mathbf{q})}{\partial \mathbf{q}_V} & \frac{\partial \mathbf{h}(\mathbf{q})}{\partial d_1} & \frac{\partial \mathbf{h}(\mathbf{q})}{\partial d_2} & \frac{\partial \mathbf{h}(\mathbf{q})}{\partial d_3} \end{bmatrix} \in \mathbb{R}^{6 \times 6},$$

is a square matrix, hence this system is square, too.

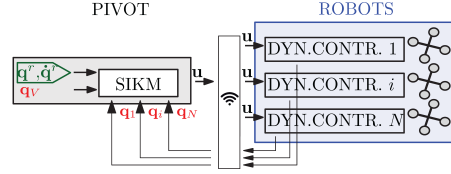
The previous examples show that the considered class of square systems includes many relevant applications.



(a) Decentralized (no communication) control (4).



(b) Distributed communication control (5).



(c) Centralized communication control (6).

Fig. 4. Controller architectures for trajectory tracking. The pivot is colored in gray, each robot (equipped with a dynamical controller which converts \mathbf{u} to forces) in blue, sensor measurements in red, and the reference trajectory in green. The wireless symbol refers to sampled communication.

3 Control Architectures

We consider a tracking problem where a multi-robot system is required to follow a sequence of desired configurations assigned *a priori*. We assume that such reference trajectory is generated offline by a high-level planner that takes into account goals such as obstacle avoidance, singular points, and energy minimization. Also, we assume that robots are equipped with dynamical controllers sufficiently fast w.r.t. the dynamics of the system, such that (s.t.) their velocities are fully controllable,

$$\dot{\mathbf{p}}(t) = \mathbf{u}(t), \quad (3)$$

where $\mathbf{u} = [\mathbf{u}_1^\top \ \dots \ \mathbf{u}_N^\top]^\top \in \mathbb{R}^n$. We now enumerate possible control architectures to achieve trajectory tracking.

Decentralized (no communication) control. A commonly adopted architecture is the following *fully decentralized* controller,

$$\mathbf{u}_i(t) = \kappa_i^{\text{dec}}(\mathbf{p}_i(t); \mathbf{p}_i^r(t), \dot{\mathbf{p}}_i^r(t)). \quad (4)$$

In this case, each robot needs only local position measurements $\mathbf{p}_i(t)$ (no configuration variables $\mathbf{q}(t)$ are needed) to implement feedback and follow its reference trajectory $(\mathbf{p}_i^r(t), \dot{\mathbf{p}}_i^r(t))$, namely, controller (4) is

communication-less and the control design reduces to a distributed planning problem (Fig. 4a). A typical example is $\mathbf{u}_i(t) = -k(\mathbf{p}_i(t) - \mathbf{p}_i^r(t)) + \dot{\mathbf{p}}_i^r(t)$. However, lacking communication and coordination, strategy (4) is not robust against disturbances or robot failures/biases.

Distributed communication control. A distributed controller reads

$$\mathbf{u}_i(t) = \kappa_i^{\text{distr}}(\mathbf{q}_i(t), \mathbf{q}_V(hT); \mathbf{q}_i^r(t), \mathbf{q}_V^r(t), \dot{\mathbf{q}}_i^r(t), \dot{\mathbf{q}}_V^r(t)), \quad (5)$$

where $t \in [hT, (h+1)T)$, $h \in \mathbb{N}$. Specifically, $\mathbf{u}_i(t)$ depends on the robot's own configuration $\mathbf{q}_i(t)$, which can be measured at all times, and on the load configuration $\mathbf{q}_V(hT)$, which is transmitted via wireless and available at discrete time instants hT , T being the sampling time. Also, reference trajectories of robot ($\mathbf{q}_i^r(t), \dot{\mathbf{q}}_i^r(t)$) and load ($\mathbf{q}_V^r(t), \dot{\mathbf{q}}_V^r(t)$) are continuously available as they are computed offline and pre-stored on robots. Hence, controller (5) implements a *hybrid continuous-sampled* control that includes both continuous-time and discrete-time signals, inducing more challenging design (Fig. 4b).

Centralized control. Lastly, the centralized controller

$$\mathbf{u}_i(t) = \kappa_i^{\text{centr}}(\mathbf{q}(hT); \mathbf{q}^r(t), \dot{\mathbf{q}}^r(t)) \quad (6)$$

depends on the full system configuration vector $\mathbf{q}(hT)$. Figure 4c shows a possible implementation where the controller, located on the pivot, receives all measurements $\mathbf{q}(t)$ and broadcasts the control input $\mathbf{u}(t)$ to the robots via wireless. In this case, while performance is theoretically maximized, all-to-all communication burden may cause issues through limitations of wireless communication in terms of bandwidth and reliability.

3.1 Proposed SIKM Architectures

In this paper, we focus on the two communication-based approaches. While these are attractive by virtue of robustness properties, their design gets challenging when shifting from continuous-time (typically assumed in the literature) to hybrid continuous- and discrete-time dynamics. In particular, the presence of sampled measurements in (5)–(6) makes both controller design and stability analysis nontrivial.

Indeed, for continuous-time systems, the controller [28]

$$\mathbf{u}(t) = \underbrace{-k\mathbf{A}_{\mathbf{q}(t)}(\mathbf{q}(t) - \mathbf{q}^r)}_{:=\mathbf{u}_k(t)} + \underbrace{\mathbf{A}_{\mathbf{q}(t)}\dot{\mathbf{q}}^r(t)}_{:=\mathbf{u}_{ff}(t)} \quad (7)$$

drives the system configuration $\mathbf{q}(t)$ to the desired reference trajectory $\mathbf{q}^r(t)$ exponentially fast, whereby the tracking error $\mathbf{e}(t) \stackrel{\text{def}}{=} \mathbf{q}(t) - \mathbf{q}^r(t)$ obeys dynamics

$$\dot{\mathbf{e}}(t) = \dot{\mathbf{q}}(t) - \dot{\mathbf{q}}^r(t) = -k(\mathbf{q}(t) - \mathbf{q}^r(t)) = -k\mathbf{e}(t).$$

Moreover, in light of (2), the centralized controller (7) can be implemented with a distributed architecture,

$$\begin{aligned} \mathbf{u}_i(t) = & -k\mathbf{A}_{\mathbf{q}_i(t)}^{(i)}(\mathbf{q}_i(t) - \mathbf{q}_i^r(t)) + \mathbf{A}_{\mathbf{q}_i(t)}^{(i)}\dot{\mathbf{q}}_i^r(t) \\ & - k\mathbf{A}_{\mathbf{q}_V(t)}^{(i)}(\mathbf{q}_V(t) - \mathbf{q}_V^r(t)) + \mathbf{A}_{\mathbf{q}_V(t)}^{(i)}\dot{\mathbf{q}}_V^r(t). \end{aligned} \quad (8)$$

When measurements are sampled, suitably modifying (7) is nontrivial. In [24], the authors proposed the following feedback controller for point-stabilization,

$$\mathbf{u}(t) = \mathbf{u}_k(hT) = -k\mathbf{A}_{\mathbf{q}(hT)}(\mathbf{q}(hT) - \mathbf{q}^r), \quad (9)$$

for $t \in [hT, (h+1)T)$. A common strategy for trajectory tracking in robotic applications is sampling (9),

$$\mathbf{u}(t) = \mathbf{u}_k(hT) = -k\mathbf{A}_{\mathbf{q}(hT)}(\mathbf{q}(hT) - \mathbf{q}^r(hT)), \quad (10)$$

which however cannot guarantee perfect tracking under nominal conditions because it lacks feedforward correction (see Appendix B for details).

A naive attempt to improve (10) is sampling (7),

$$\begin{aligned} \mathbf{u}(hT + \tau) = & -k\mathbf{A}_{\mathbf{q}(hT)}(\mathbf{q}(hT) - \mathbf{q}^r(hT)) \\ & + \mathbf{A}_{\mathbf{q}(hT)}\dot{\mathbf{q}}^r(hT + \tau), \quad \tau \in [0, T), \end{aligned} \quad (11)$$

which results in the following error dynamics,

$$\begin{aligned} \dot{\mathbf{e}}(hT + \tau) = & -k\mathbf{A}_{\mathbf{e}(hT+\tau)+\mathbf{q}^r(hT+\tau)}^{-1}\mathbf{A}_{\mathbf{e}(hT)+\mathbf{q}^r(hT)}\mathbf{e}(hT) + \\ & + (\mathbf{A}_{\mathbf{e}(hT+\tau)+\mathbf{q}^r(hT+\tau)}^{-1}\mathbf{A}_{\mathbf{e}(hT)+\mathbf{q}^r(hT)} - \mathbf{I})\dot{\mathbf{q}}^r(hT + \tau). \end{aligned}$$

It is indeed easy to show that, under controller (11), reference $\mathbf{q}^r(t)$ is not an equilibrium trajectory, making also the latter attempt not suitable for trajectory tracking.

Proposition 1 *Under control strategy (11), the reference trajectory is not an equilibrium trajectory, i.e.,*

$$\mathbf{q}(t) = \mathbf{q}^r(t) \not\Rightarrow \dot{\mathbf{e}}(t) = 0, \forall t \geq 0.$$

PROOF. If $\mathbf{q}(t) = \mathbf{q}^r(t)$, then $\mathbf{e}(t) = 0$ and

$$\dot{\mathbf{e}}(hT + \tau) = (\mathbf{A}_{\mathbf{q}^r(hT+\tau)}^{-1}\mathbf{A}_{\mathbf{q}^r(hT)} - \mathbf{I})\dot{\mathbf{q}}^r(hT + \tau),$$

which is nonzero for all $h \in \mathbb{N}$ and $\tau \in (0, T)$ unless $\dot{\mathbf{q}}^r(t) \equiv \mathbf{0}$, i.e., the reference trajectory is constant. \square

Finally, we modify controller (11) as follows,

$$\begin{aligned} \mathbf{u}(hT + \tau) = & -k\mathbf{A}_{\mathbf{q}(hT)}(\mathbf{q}(hT) - \mathbf{q}^r(hT)) \\ & + \mathbf{A}_{\mathbf{q}^r(hT+\tau)}\dot{\mathbf{q}}^r(hT + \tau), \quad \tau \in [0, T). \end{aligned} \quad (12)$$

Differently from (11), the Jacobian of the feedforward term in (12) is computed at $\mathbf{q}^r(hT+\tau)$ instead of $\mathbf{q}(hT)$. Accordingly, the error dynamics become

$$\begin{aligned} \dot{\mathbf{e}}(hT+\tau) &= -k\mathbf{A}_{\mathbf{e}(hT+\tau)+\mathbf{q}^r(hT+\tau)}^{-1}\mathbf{A}_{\mathbf{e}(hT)+\mathbf{q}^r(hT)}\mathbf{e}(hT)+ \\ &\quad +(\mathbf{A}_{\mathbf{e}(hT+\tau)+\mathbf{q}^r(hT+\tau)}^{-1}\mathbf{A}_{\mathbf{q}^r(hT+\tau)}-\mathbf{I})\dot{\mathbf{q}}^r(hT+\tau) \\ &\stackrel{\text{def}}{=} \mathbf{f}(\mathbf{e}(hT+\tau), \mathbf{q}^r(hT+\tau), \dot{\mathbf{q}}^r(hT+\tau)), \end{aligned} \quad (13)$$

whereby the reference can be shown to be an equilibrium trajectory.

Proposition 2 *Under control strategy (12) the reference trajectory $\mathbf{q}^r(t)$ is an equilibrium trajectory, i.e.,*

$$\mathbf{q}(t) = \mathbf{q}^r(t) \Rightarrow \dot{\mathbf{e}}(t) = 0, \forall t \geq 0.$$

PROOF. If $\mathbf{q}(t) = \mathbf{q}^r(t)$, then $\mathbf{e}(t) \equiv 0$ and

$$\dot{\mathbf{e}}(hT+\tau) = (\mathbf{A}_{\mathbf{q}^r(hT+\tau)}^{-1}\mathbf{A}_{\mathbf{q}^r(hT+\tau)}-\mathbf{I})\dot{\mathbf{q}}^r(hT+\tau) \equiv 0. \quad \square$$

Also, by virtue of the assumed structure (2) of the Jacobian, controller (12) can be decoupled and is thus amenable of a distributed communication implementation of the form (5),

$$\begin{aligned} \mathbf{u}_i(hT+\tau) &= -k\mathbf{A}_{\mathbf{q}_i(hT)}^{(i)}(\mathbf{q}_i(hT)-\mathbf{q}_i^r(hT)) \\ &\quad -k\mathbf{A}_{\mathbf{q}_V(hT)}^{(i)}(\mathbf{q}_V(hT)-\mathbf{q}_V^r(hT)) \\ &\quad +\mathbf{A}_{\mathbf{q}_i^r(hT+\tau)}^{(i)}\dot{\mathbf{q}}_i^r(hT+\tau) \\ &\quad +\mathbf{A}_{\mathbf{q}_V^r(hT+\tau)}^{(i)}\dot{\mathbf{q}}_V^r(hT+\tau). \end{aligned} \quad (14)$$

In the following, we analyze system dynamics under controller (12) to evaluate stability and performance. In view of (14), all results straightly carry over to a distributed architecture. Furthermore, in simulation we will test the centralized controller where the feedback gain k is adaptive: this cannot be decoupled, because computing k online requires the full system configuration.

4 Stability Limitations of SIKM

In this section we prove a negative result: perfect nominal tracking cannot be ensured for some values of (k, T) . In particular, the gain k needs to be sufficiently large and the sampling time T sufficiently small to avoid instability. To this aim, we state some preliminary assumptions.

Assumption 1 *The following relations hold.*

- i) The reference trajectory $\mathbf{q}^r(t) \in \mathcal{Q}$ is twice continuously differentiable and \mathcal{Q} is a compact set. Moreover, velocities and accelerations are uniformly bounded, i.e., $\|\dot{\mathbf{q}}^r(t)\| \leq v_{max}$ and $\|\ddot{\mathbf{q}}^r(t)\| \leq a_{max}$.*

- ii) $\mathbf{A}_{\mathbf{q}(0)}$ is twice continuously differentiable and invertible.*

- iii) There exists $d > 0$ such that, for any configuration \mathbf{q} at distance smaller than d from the reference trajectory, i.e., $\exists t : \|\mathbf{q} - \mathbf{q}^r(t)\| < d$, $\mathbf{A}_{\mathbf{q}}$ is twice continuously differentiable and invertible.*

Assumption 1-i) are smoothness properties of the reference trajectory needed to derive error bounds. Assumption 1-ii) is required to avoid that the initial condition is a singular point. Assumption 1-iii) further guarantees that all configurations $\mathbf{q}^r(t)$ belonging to the reference trajectory are distant enough from singular points, ensuring robustness to, e.g., external disturbances, and can be accommodated through an offline high-level planner. We will later show that our proposed control strategies, under such assumptions, also guarantees that the actual trajectory is always bounded away from singular points.

The error flow $\mathbf{f}(\cdot, \cdot, \cdot)$ in (14) is discontinuous because the feedback term depends on $\mathbf{e}(hT)$ and resets at every sampling instant $t = hT$. Thus, existence of a global solution based on standard Lipschitz continuity cannot be invoked, in general. However, in view of Assumption 1, the flow is Lipschitz continuous for $\tau \in [0, T)$. Hence, if we can show that a solution $\mathbf{e}(hT + \tau)$ exists for any $\tau \in [0, T)$, and that the limit $\lim_{\tau \rightarrow T} \mathbf{e}(hT + \tau)$ exists finite starting from any $\mathbf{e}(hT)$ satisfying Assumption 1, then global existence is guaranteed by patching together those intervals. As so, we study the flow $\mathbf{f}(\mathbf{e}(t), \mathbf{q}^r(t), \dot{\mathbf{q}}^r(t); \mathbf{e}(hT))$ for $t = hT + \tau$, $\tau \in [0, T)$, where we make the dependence on the ‘‘initial condition’’ $\mathbf{e}(hT)$ explicit. To prove asymptotic stability, we will use the following notion of contraction.

Definition 3 *Given fixed T, k , and under Assumption 1, the flow $\mathbf{f}(\mathbf{e}(t), \mathbf{q}^r(t), \dot{\mathbf{q}}^r(t); \mathbf{e}(hT))$ is ρ -monotonically contractive if, for any $\|\mathbf{e}(hT)\| < d$, it holds*

- (1) $\|e(hT + \tau)\| \leq \|e(hT)\|$, $\tau \in [0, T)$,*
- (2) $\lim_{\tau \rightarrow T} \|e(hT + \tau)\| \leq \rho \|e(hT)\|$, $\rho \in [0, 1)$.*

Given Definition 3, the following lemma easily follows.

Lemma 4 *If the error flow defined in (13) is ρ -monotonically contractive and under Assumption 1, then*

$$\|\mathbf{q}(t) - \mathbf{q}^r(t)\| \leq \rho^{\frac{t}{T}-1} \|\mathbf{q}(0) - \mathbf{q}^r(0)\|, \quad t \geq 0.$$

Lemma 4 ensures exponential convergence to the reference trajectory. The property of ρ -monotonically contractiveness might appear rather strong since it must hold for any segment of the trajectory of length T , however, it is necessary to guarantee that the system avoids singularity configurations at all times. The next result encodes necessary conditions for stability.

Proposition 5 Under Assumption 1, there exists $k_{min} > 0$ such that, if one of the following conditions is satisfied,

- (1) $k < k_{min}$,
- (2) $k > \frac{2}{T}$,

the error flow (13) is not ρ -monotonically contractive.

Intuitively, if the gain k is too small, there exist reference trajectories such that the feedforward term “pushes” the system too much without being suitably balanced by the feedback term. Conversely, if k is too large, the feedback causes the trajectory to overshoot, possibly amplifying the error of the initial condition.

PROOF. 1) We will prove the first condition showing that the error norm initially increases for some initial conditions $\mathbf{e}(hT)$ and choice of reference trajectory $\mathbf{q}^r(t)$. Consider the following Lyapunov function

$$V(\tau) = \frac{1}{2} \|\mathbf{e}(hT + \tau)\|^2, \quad (15)$$

and its time derivative at $\tau = 0$ (cf. (13)):

$$\begin{aligned} \dot{V}(0) &= \mathbf{e}(hT)^\top \dot{\mathbf{e}}(hT) \\ &= -k \|\mathbf{e}(hT)\|^2 + \\ &\quad \underbrace{\mathbf{e}^\top(hT) (\mathbf{A}_{\mathbf{e}(hT) + \mathbf{q}^r(hT)}^{-1} \mathbf{A}_{\mathbf{q}^r(hT)} - \mathbf{I}) \dot{\mathbf{q}}^r(hT)}_{\stackrel{\text{def}}{=} \phi(\mathbf{e}(hT), \mathbf{q}^r(hT), \dot{\mathbf{q}}^r(hT))}. \end{aligned}$$

Let us define

$$\begin{aligned} c_{max} &\stackrel{\text{def}}{=} \max c \\ \text{s.t.} \quad &\|\mathbf{e}(hT)\| \leq d, \mathbf{q}^r(hT) \in \mathcal{Q}, \\ &\phi(\mathbf{e}(hT), \mathbf{q}^r(hT), \dot{\mathbf{q}}^r(hT)) \geq cv_{max} \|\mathbf{e}(hT)\|^2. \end{aligned}$$

The parameter c_{max} is surely strictly positive because (i) all arguments of $\phi(\cdot)$ are defined on a compact set (see also Assumption 1-i) and (ii) $\phi(\cdot)$ is continuously differentiable. The only case for which $c_{max} = 0$ is when $\mathbf{A}_{\mathbf{q}}$ is a constant matrix for all \mathbf{q} . This scenario is not admissible since it would imply $\dot{\mathbf{p}} = \mathbf{A}\dot{\mathbf{q}}$, which is not the case for the problem at hand. This implies that there exist tuples $(\mathbf{e}(hT), \mathbf{q}^r(hT), \dot{\mathbf{q}}^r(hT))$ such that

$$\dot{V}(0) \geq -(k - c_{max}v_{max}) \|\mathbf{e}(hT)\|^2$$

Let $k_{min} \stackrel{\text{def}}{=} c_{max}v_{max}$, then $\dot{V}(0) > 0$ for any $k < k_{min}$, hence there exists $0 < \bar{\tau} < T$ s.t. $\|\mathbf{e}(hT + \tau)\| > \|\mathbf{e}(hT)\| \forall \tau \in (0, \bar{\tau})$ and (13) it is not ρ -monotonically contractive.

2) In order to prove the second condition we first choose $\mathbf{q}^r(t) \equiv \mathbf{q}^r$, $t \geq 0$, which satisfies Assumption 1. As so, the error dynamics reduce to

$$\dot{\mathbf{e}}(hT + \tau) = -k \underbrace{\mathbf{A}_{\mathbf{e}(hT + \tau) + \mathbf{q}^r}^{-1} \mathbf{A}_{\mathbf{e}(hT) + \mathbf{q}^r}}_{\stackrel{\text{def}}{=} \mathbf{g}(\mathbf{e}(hT + \tau))} \mathbf{e}(hT).$$

The error trajectory can be written in the form

$$\mathbf{e}(hT + \tau) = \mathbf{e}(hT) + k \int_{hT}^{hT + \tau} \mathbf{g}(\mathbf{e}(hT + \tau')) d\tau'.$$

By using Taylor’s theorem for multivariate functions with integral form of the remainder, it becomes

$$\begin{aligned} \mathbf{e}(hT + \tau) &= \mathbf{e}(hT) + k\tau \mathbf{g}(\mathbf{e}(hT)) + \\ &+ k^2\tau^2 \int_0^1 (1 - \varepsilon) \frac{\partial \mathbf{g}(\mathbf{e}(hT + \varepsilon\tau))}{\partial \mathbf{e}} \mathbf{g}(\mathbf{e}(hT + \varepsilon\tau)) d\varepsilon \\ &= (1 - k\tau) \mathbf{e}(hT) + k^2\tau^2 \mathbf{r}(\mathbf{e}(hT + \tau); \mathbf{e}(hT)), \quad (16) \end{aligned}$$

where $\mathbf{r}(\cdot)$ is the second-order reminder where we made explicit the dependence on $\mathbf{e}(hT)$. Under Assumption 1, the functions \mathbf{g} and $\frac{\partial \mathbf{g}}{\partial \mathbf{e}}$ are continuously differentiable. Moreover their arguments are defined in a compact set and have the additional properties that $\mathbf{g}(\mathbf{e}(hT + \tau)) = 0$, $\frac{\partial \mathbf{g}(hT + \tau)}{\partial \mathbf{e}} = \mathbf{0}$, $\forall \tau \in [0, T]$ if $\mathbf{e}(hT) = \mathbf{0}$. Therefore, applying Lemma A.3, there must exist $\delta > 0$ such that

$$\|\mathbf{r}(\mathbf{e}(hT + \tau); \mathbf{e}(hT))\| \leq \delta \|\mathbf{e}(hT)\|^2, \quad \forall \tau \in [0, T], \forall \mathbf{e}(hT).$$

We now use the reverse triangle inequality and the previous inequality to get:

$$\begin{aligned} \|\mathbf{e}(hT + \tau)\| &\geq \\ &\geq \|(1 - k\tau) \mathbf{e}(hT)\| - k^2\tau^2 \|\mathbf{r}(\mathbf{e}(hT + \tau); \mathbf{e}(hT))\| \\ &\geq \max\{0, |1 - k\tau| - k^2\tau^2\delta\} \|\mathbf{e}(hT)\|. \end{aligned}$$

If $kT > 2$, there exist $\epsilon > 0$ and $\bar{\tau} \in (0, T)$ s.t. $k\bar{\tau} = 2 + \epsilon$. Then, we can choose $\mathbf{e}(hT)$ s.t. $\|\mathbf{e}(hT)\| = \frac{\epsilon}{2k\bar{\tau}^2\delta}$, hence

$$\|\mathbf{e}(hT + \bar{\tau})\| \geq \left(1 + \epsilon - \frac{\epsilon}{2}\right) \|\mathbf{e}(hT)\| \geq \|\mathbf{e}(hT)\|. \quad \square$$

Remark 6 (Stability limitations on T and k)

Proposition 5 states that there are choices of T and k for which the error flow (13) is not ρ -monotonically contractive, implying that the robots may not track the reference trajectory. In particular, there exists a feedback gain k_{min} below which the system cannot be ρ -monotonically contractive. Also, there exists a sampling time $T_{max} = \frac{2}{k_{min}}$ above which the same instability consideration applies, as graphically shown in Fig. 1. This is in stark contrast with the result for position stabilization in [24], where (doubly) exponential stability could be achieved without sharp limitation on sampling time T or control gain k .

This fundamental difference is mainly due to the novel feedforward term considered in this work.

The previous negative results entails necessary conditions on k and T for stability. Conversely, we next prove that there exist pairs of T and k for which ρ -monotonically contractiveness holds.

Proposition 7 *Under Assumption 1, there exists $k_2 > 0$ such that for any $k > k_2$ there exists $T_c(k)$ such that for all $T < T_c(k)$ the error flow defined in (13) is ρ -monotonically contractive.*

PROOF. Consider the Lyapunov function (15) and its time derivative at $\tau = 0$:

$$\begin{aligned} \dot{V}(0) &= -k\|\mathbf{e}(hT)\|^2 + \\ &+ \mathbf{e}^\top(hT)(\mathbf{A}_{\mathbf{e}(hT)+\mathbf{q}^r(hT)}^{-1}\mathbf{A}_{\mathbf{q}^r(hT)} - \mathbf{I})\dot{\mathbf{q}}^r(hT). \end{aligned}$$

Note that $\mathbf{A}_{\mathbf{e}(hT)+\mathbf{q}^r(hT)}^{-1}\mathbf{A}_{\mathbf{q}^r(hT)} - \mathbf{I} = \mathbf{0} \ \forall \mathbf{q}^r(hT)$ if $\mathbf{e}(hT) = \mathbf{0}$. Moreover, being $\mathbf{e}(hT)$ and $\mathbf{q}^r(hT)$ in a compact set according to Assumption 1, by virtue of Lemma A.2 it holds $\|\mathbf{A}_{\mathbf{e}(hT)+\mathbf{q}^r(hT)}^{-1}\mathbf{A}_{\mathbf{q}^r(hT)} - \mathbf{I}\| \leq \delta\|\mathbf{e}(hT)\|$ for some $\delta > 0$, therefore

$$\begin{aligned} \dot{V}(0) &\leq -k\|\mathbf{e}(hT)\|^2 + \delta\|\mathbf{e}(hT)\|^2 v_{max} \\ &= -(k - \delta v_{max})\|\mathbf{e}(hT)\|^2 = -2(k - \delta v_{max})V(0). \end{aligned}$$

Let $k_2 \stackrel{\text{def}}{=} \delta v_{max}$, then for each $k > k_2$, there exist $\xi \in (0, k - \delta v_{max})$ and $T_c(k)$ s.t.

$$\begin{aligned} V(\tau) &\leq e^{-2\xi\tau}V(0), \tau \in [0, T_c(k)] \\ \implies \|\mathbf{e}(hT + \tau)\| &\leq e^{-\xi\tau}\|\mathbf{e}(hT)\|, \tau \in [0, T_c(k)]. \end{aligned}$$

As a consequence, by defining $\rho \stackrel{\text{def}}{=} e^{-T\xi} < 1$ for any $T < T_c(k)$, it holds

$$\begin{aligned} \|\mathbf{e}(hT + \tau)\| &\leq \rho\|\mathbf{e}(hT)\|, \tau \in [0, T) \\ \lim_{\tau \rightarrow T} \|\mathbf{e}(hT + \tau)\| &\leq \rho\|\mathbf{e}(hT)\|, \end{aligned}$$

i.e., the system is ρ -monotonically contractive. \square

By combining this result with the previous one, it follows that $\lim_{k \rightarrow \infty} T_c(k) = 0$ and that $T_c(k) < T_{max} \ \forall k > k_2$. From Proposition 5, we know that (13) is not ρ -monotonically contractive for values of (k, T) in the red area of Fig. 1. Conversely, Proposition 7 asserts that there exist a non-empty area within the parameter space, represented by the white area below the dashed red curve in Fig. 1, such that (13) is ρ -monotonically contractive.

In the next section, we explicitly compute a bounded area in the (k, T) -space that guarantees ρ -monotonic

contractiveness of (13), and hence perfect asymptotic tracking under nominal conditions.

5 Stability and Convergence Rate for SIKM

All results in the previous section are of existential type, i.e., they give no indication about computing the pairs k and T for which the system is ρ -monotonically contractive, nor the convergence rate ρ . In this section, we find explicit bounds on the “stability” set (green area in Fig. 1) where the error norm decreases. Also, we characterize the convergence rate and find the pairs of gain and sampling time that induce the fastest convergence.

Remark 8 (Stability) *When mentioning stability, we imply that the flow (13) is ρ -monotonically contractive.*

Proposition 9 *For system (13), it is possible to upper bound the decrease rate of the error norm $\|\mathbf{e}(\cdot)\|$,*

$$\|\mathbf{e}(hT + \tau)\| \leq z(k, \tau; \mu, \alpha, \gamma_1, \gamma_2) \cdot \|\mathbf{e}(hT)\|, \quad (17)$$

for $h \in \mathbb{N}$, $\tau \in (0, \tau_s(k))$, and

$$z(k, \tau; \mu, \alpha, \gamma_1, \gamma_2) = |1 - k\tau| + \tau\alpha + \tau^2(k^2\mu + k\gamma_1 + \gamma_2),$$

where $\alpha, \mu, \gamma_1, \gamma_2$ are positive constants.

PROOF. [Sketch] In virtue of the Lipschitz properties of the error flow in the interval $(hT, hT+T)$, Taylor’s theorem with integral form of the remainder for multivariate functions is used to decompose the error $\mathbf{e}(hT + \tau)$ as a sum of terms which can be upper bounded individually. Notice that α, μ, γ_1 and γ_2 are still unknown at this stage.

PROOF. The flow defined by (13) can be written as

$$\mathbf{e}(hT + \tau) = \mathbf{e}(hT) + \int_{hT}^{hT + \tau} \mathbf{f}(\mathbf{e}(\cdot), \mathbf{q}^r(\cdot), \dot{\mathbf{q}}^r(\cdot)) \Big|_{hT + \tau'} d\tau'.$$

By using Taylor’s theorem for multivariate functions with integral form of the remainder, we get

$$\begin{aligned} \mathbf{e}(hT + \tau) &= \mathbf{e}(hT) + \tau \mathbf{f}(\mathbf{e}(hT), \mathbf{q}^r(hT), \dot{\mathbf{q}}^r(hT)) + \\ &+ \tau^2 \int_0^1 (1 - \varepsilon) \cdot \left[\frac{\partial \mathbf{f}(\mathbf{e}(\cdot), \mathbf{q}^r(\cdot), \dot{\mathbf{q}}^r(\cdot))}{\partial \mathbf{e}(\cdot)} \mathbf{f}(\mathbf{e}(\cdot), \mathbf{q}^r(\cdot), \dot{\mathbf{q}}^r(\cdot)) + \right. \\ &+ \frac{\partial \mathbf{f}(\mathbf{e}(\cdot), \mathbf{q}^r(\cdot), \dot{\mathbf{q}}^r(\cdot))}{\partial \mathbf{q}^r(\cdot)} \dot{\mathbf{q}}^r(\cdot) + \\ &\left. + \frac{\partial \mathbf{f}(\mathbf{e}(\cdot), \mathbf{q}^r(\cdot), \dot{\mathbf{q}}^r(\cdot))}{\partial \dot{\mathbf{q}}^r(\cdot)} \ddot{\mathbf{q}}^r(\cdot) \right]_{hT + \varepsilon\tau} d\varepsilon. \quad (18) \end{aligned}$$

The above expression allows to find an upper bound of $\|\mathbf{e}(hT + \tau)\|$, $\tau \in (0, \tau_s(k))$, by acting on the single terms

of (18). Hence, we can compute a more precise estimate of the convergence rate, i.e., how quickly $\|\mathbf{e}(hT + \tau)\|$, with $\tau \in (0, \tau_s(k))$, decreases w.r.t. $\|\mathbf{e}(hT)\|$. Moreover, the following computations will be useful to find values (k, T) s.t. the system is stable and the tracking error converges to zero. First, we observe that

$$\begin{aligned} \mathbf{f}(\mathbf{e}(hT), \mathbf{q}^r(hT), \dot{\mathbf{q}}^r(hT)) &= -k\mathbf{e}(hT) + \\ &+ (\mathbf{A}_{\mathbf{e}(hT)+\mathbf{q}^r(hT)}^{-1} \mathbf{A}_{\mathbf{q}^r(hT)} - \mathbf{I}) \dot{\mathbf{q}}^r(hT). \end{aligned} \quad (19)$$

By using Lemma A.2 on the second addend, it holds

$$\|(\mathbf{A}_{\mathbf{e}(hT)+\mathbf{q}^r(hT)}^{-1} \mathbf{A}_{\mathbf{q}^r(hT)} - \mathbf{I}) \dot{\mathbf{q}}^r(hT)\| \leq \alpha \|\mathbf{e}(hT)\|,$$

where $\alpha \stackrel{\text{def}}{=} av_{max}$ for some $a > 0$ that depends on the system dynamics. Moreover, from (13),

$$\begin{aligned} \|\mathbf{f}(\mathbf{e}(hT + \tau), \mathbf{q}^r(hT + \tau), \dot{\mathbf{q}}^r(hT + \tau))\| &\leq \\ &\leq \| -k\mathbf{A}_{\mathbf{e}(hT+\tau)+\mathbf{q}^r(hT+\tau)}^{-1} \mathbf{A}_{\mathbf{e}(hT)+\mathbf{q}^r(hT)} \mathbf{e}(hT) \| + \\ &+ \| (\mathbf{A}_{\mathbf{e}(hT+\tau)+\mathbf{q}^r(hT+\tau)}^{-1} \mathbf{A}_{\mathbf{q}^r(hT+\tau)} - \mathbf{I}) \dot{\mathbf{q}}^r(hT + \tau) \|. \end{aligned} \quad (20)$$

Both addends in (20) are continuously differentiable functions on a compact set. In addition, they are equal to zero if $\mathbf{e}(hT) = \mathbf{0}$ and $\mathbf{e}(hT + \tau) = \mathbf{0}$, respectively. Then, we can apply Lemmas A.1-A.2 to get $\|k\mathbf{A}_{\mathbf{e}(hT+\tau)+\mathbf{q}^r(hT+\tau)}^{-1} \mathbf{A}_{\mathbf{e}(hT)+\mathbf{q}^r(hT)} \mathbf{e}(hT)\| \leq kb\|\mathbf{e}(hT)\|$, $b > 0$, and $\|(\mathbf{A}_{\mathbf{e}(hT+\tau)+\mathbf{q}^r(hT+\tau)}^{-1} \mathbf{A}_{\mathbf{q}^r(hT+\tau)} - \mathbf{I}) \dot{\mathbf{q}}^r(hT + \tau)\| \leq c\|\mathbf{e}(hT)\|v_{max}$, $c > 0$, where we used Proposition 7 and Definition 3 and constants b, c depend on the system dynamics. Thus, we rewrite (20) as

$$\|\mathbf{f}(\mathbf{e}(\cdot), \mathbf{q}^r(\cdot), \dot{\mathbf{q}}^r(\cdot))\|_{hT+\tau} \leq (kb + cv_{max})\|\mathbf{e}(hT)\|. \quad (21)$$

Also, being $\mathbf{f}(\mathbf{e}(\cdot), \mathbf{q}^r(\cdot), \dot{\mathbf{q}}^r(\cdot))$ differentiable w.r.t. all its variables on the compact set $\mathcal{B}_r(\mathbf{e}(\cdot))$, we can derive the following bounds based on (19) :

$$\begin{aligned} \left\| \frac{\partial \mathbf{f}(\mathbf{e}(\cdot), \mathbf{q}^r(\cdot), \dot{\mathbf{q}}^r(\cdot))}{\partial \mathbf{e}} \right\|_{hT+\tau} &\leq (k + gv_{max})\|\mathbf{e}(hT)\| \\ \left\| \frac{\partial \mathbf{f}(\mathbf{e}(\cdot), \mathbf{q}^r(\cdot), \dot{\mathbf{q}}^r(\cdot))}{\partial \mathbf{q}^r} \right\|_{hT+\tau} &\leq mv_{max}\|\mathbf{e}(hT)\| \\ \left\| \frac{\partial \mathbf{f}(\mathbf{e}(\cdot), \mathbf{q}^r(\cdot), \dot{\mathbf{q}}^r(\cdot))}{\partial \dot{\mathbf{q}}^r} \right\|_{hT+\tau} &\leq kn\|\mathbf{e}(hT)\|, \end{aligned} \quad (22)$$

where $g, m, n > 0$ also depend on the system dynamics. In virtue of (19), (21) and (22), we can derive the overall bound defined in (17):

$$\|\mathbf{e}(hT + \tau)\| \leq (|1 - k\tau| + \alpha\tau + \tau^2(k^2\mu + k\gamma_1 + \gamma_2))\|\mathbf{e}(hT)\|$$

where, given $a > 0$ defined in the proof of Proposition 5,

$$\begin{aligned} \alpha &\stackrel{\text{def}}{=} av_{max} \\ \mu &\stackrel{\text{def}}{=} b\|\mathbf{e}(hT)\| \\ \gamma_1 &\stackrel{\text{def}}{=} (c + gb)v_{max}\|\mathbf{e}(hT)\| + na_{max} \\ \gamma_2 &\stackrel{\text{def}}{=} gc v_{max}\|\mathbf{e}(hT)\| + m v_{max}. \quad \square \end{aligned}$$

Proposition 9 provides an expression for the convergence rate as a function of the parameters $\mu, \alpha, \gamma_1, \gamma_2$. In the next section, we provide a procedure to estimate them.

Remark 10 (Constant reference) Consider (17) and suppose a constant reference is assigned, i.e., $\frac{d^{(n)}\mathbf{q}^r(t)}{dt^{(n)}} \equiv \mathbf{0}$, $n \geq 1$. Then $\alpha = \gamma_1 = \gamma_2 = 0$ and $z(k, \tau; \mu)$ coincides with the function $g(\tau; \mu)|_{\tau=k\tau}$ found in [24].

5.1 Estimating Parameters $\mu, \alpha, \gamma_1, \gamma_2$

We would like to find an estimate of the function $z(k, \tau; \mu, \alpha, \gamma_1, \gamma_2)$ that bounds the convergence rate of the tracking error, and choose the values (k, T) which yield the fastest convergence. To this aim, we provide a numerical procedure to estimate $\theta \stackrel{\text{def}}{=} (\mu, \alpha, \gamma_1, \gamma_2)$. Proposition 9 implies that the following set is nonempty,

$$\Theta \stackrel{\text{def}}{=} \{\theta > 0 \mid \|\mathbf{e}(hT + \tau)\| \leq z(k, \tau; \theta)\|\mathbf{e}(hT)\|, \forall \mathbf{q}^r(\cdot), \mathbf{q}(0)\},$$

where the inequality is componentwise. Ideally, we would like to pick the smallest possible values for the parameters in θ in order to get the largest set of pairs (k, T) that induce stability. One possibility is choosing

$$\vartheta \stackrel{\text{def}}{=} \underset{\theta \in \Theta}{\text{argmin}} \|\theta\|.$$

Such ϑ surely exists because $\mathbf{q}^r(\cdot)$ and $\mathbf{q}(0)$ belong to a compact set. However, it cannot be computed numerically because one would need to check all pairs (k, T) and points $\mathbf{q}^r(t)$ and $\mathbf{q}(0)$. We propose a strategy to estimate ϑ by sampling $\mathbf{q}^r(t)$ and $\mathbf{q}(0)$ from their domains for different values of (k, T) and run simulations to get a set of samples $\{(k_i, T_i, \mathbf{e}_{h+1}^i, \mathbf{e}_h^i)\}_{i=1}^S$, S being the number of samples. Let us define the following quantities,

$$\begin{aligned} y_i &\stackrel{\text{def}}{=} \|\mathbf{e}_{h+1}^i\|, \\ s_i^\top &\stackrel{\text{def}}{=} [T_i^2 \ k_i^2 \ T_i \ T_i^2 k_i \ T_i^2] \|\mathbf{e}_h^i\| \\ b_i &\stackrel{\text{def}}{=} |1 - k_i T_i| \|\mathbf{e}_h^i\|, \end{aligned}$$

then the inequality $\|\mathbf{e}_{h+1}^i\| \leq z(k_i, T_i; \theta)\|\mathbf{e}_h^i\|$ can be written as $y_i \leq s_i^\top \theta + b_i$. Based on such sampled trajec-

tories, we solve the following quadratic programming:

$$\begin{aligned} \widehat{\theta}_S &\stackrel{\text{def}}{=} \underset{\theta}{\operatorname{argmin}} \quad \|\theta\|^2 \\ \text{s. t.} \quad &\theta \geq 0, \\ &y_i \leq s_i^\top \theta + b_i, \quad i = 1, \dots, S. \end{aligned} \quad (23)$$

Unfortunately, it is possible that $\widehat{\theta}_S \notin \Theta$ since we are checking the inequality $\|\mathbf{e}(hT + \tau)\| \leq z(k, \tau; \theta) \|\mathbf{e}(hT)\|$ over a finite number of points. We expect that $\lim_{S \rightarrow \infty} \widehat{\theta}_S = \vartheta$ if the sampling procedure covers domains of $\mathbf{q}^r(\cdot)$ and $\mathbf{q}(0)$ widely enough. However, formally proving this claim is nontrivial. There might be alternative numerical strategies to compute better estimates of ϑ , or other parameter choices in the set Θ . Such comparison goes beyond the scope of this work, however, we will show effectiveness of our proposed strategy through simulations.

5.2 Analysis of the Function $z(k, \tau; \mu, \alpha, \gamma_1, \gamma_2)$

In this section, we analyze the function $z(k, \tau)$ in order to compute the bound $\tau_s(k)$ of the stability region (green area in Fig. 1), defined as¹

$$\mathcal{U} \stackrel{\text{def}}{=} \{(k, \tau) : z(k, \tau) < 1\}, \quad (24)$$

and the convergence rate for each point in such region.

We also compute the optimal controller gain $k_o(T)$ for a fixed sampling time T and the optimal sampling time $T_s(k)$ for a fixed gain k to achieve the fastest convergence rate. Notice that $z(k, \tau; \mu, \alpha, \gamma_1, \gamma_2)$ can be written as²:

$$z(k, \tau) = \begin{cases} z^-(k, \tau) & \text{if } k\tau < 1 \\ z^+(k, \tau) & \text{if } k\tau > 1 \end{cases},$$

where

$$\begin{aligned} z^-(k, \tau) &= 1 + \tau(\alpha - k) + \tau^2(k^2\mu + k\gamma_1 + \gamma_2) \\ z^+(k, \tau) &= -1 + \tau(\alpha + k) + \tau^2(k^2\mu + k\gamma_1 + \gamma_2). \end{aligned}$$

Proposition 11 *The guaranteed stability set of $z(k, \tau)$ is*

$$\mathcal{U} = \{\alpha < k < +\infty, 0 < \tau < \tau_s(k)\},$$

¹ In the following, we use the shorthand notation $z(k, \tau) \stackrel{\text{def}}{=} z(k, \tau; \mu, \alpha, \gamma_1, \gamma_2)$ for the sake of readability.

² In the following, we use the shorthand notation $z(k, \tau) \stackrel{\text{def}}{=} z(k, \tau; \mu, \alpha, \gamma_1, \gamma_2)$ for the sake of readability.

where $\alpha = k_{\min}$ was defined in Proposition 9 and

$$\tau_s(k) = \begin{cases} \tau_{s_1}(k) & \text{if } \mu > 1 \\ \tau_{s_1}(k) & \text{for } \alpha < k < \bar{k} \quad \text{if } \mu < 1, \\ \tau_{s_2}(k) & \text{for } k > \bar{k} \quad \text{if } \mu < 1 \end{cases}$$

$$\begin{aligned} \text{where } \tau_{s_1} &\stackrel{\text{def}}{=} \frac{k - \alpha}{k^2\mu + k\gamma_1 + \gamma_2}, \quad \bar{k} \stackrel{\text{def}}{=} \frac{\alpha + \gamma_1 + \sqrt{(\alpha + \gamma_1)^2 + 4\gamma_2(1 - \mu)}}{2(1 - \mu)}, \\ \tau_{s_2} &\stackrel{\text{def}}{=} \frac{-(\alpha + k) + \sqrt{(\alpha + k)^2 + 8(k^2\mu + k\gamma_1 + \gamma_2)}}{2(k^2\mu + k\gamma_1 + \gamma_2)}. \end{aligned}$$

With fixed k , we can define the sampling time and convergence rate as functions of k :

$$\tau_o(k) \stackrel{\text{def}}{=} \underset{\tau}{\operatorname{argmin}} z(k, \tau) \quad (25)$$

$$\rho_o(k) \stackrel{\text{def}}{=} z(k, \tau_o(k)), \quad (26)$$

where τ_o is the time when $\|\mathbf{e}(hT + \tau)\|$, $0 \leq \tau \leq T$, is closest to the origin, hence it corresponds to the fastest convergence rate of the error ρ_o .

Proposition 12 *With fixed k , the optimal sampling time $\tau_o(k)$ is given by*

$$\tau_o(k) = \begin{cases} \tau_{o_1}(k) & \text{if } \mu > \frac{1}{2} \\ \tau_{o_1}(k) & \text{for } \alpha < k < \bar{k} \quad \text{if } \mu < \frac{1}{2}, \\ \frac{1}{k} & \text{for } k > \bar{k} \quad \text{if } \mu < \frac{1}{2} \end{cases}$$

$$\begin{aligned} \tau_{o_1}(k) &\stackrel{\text{def}}{=} \frac{k - \alpha}{2(k^2\mu + k\gamma_1 + \gamma_2)}, \quad \bar{k} \stackrel{\text{def}}{=} \frac{\alpha + 2\gamma_1 + \sqrt{(\alpha + 2\gamma_1)^2 + 8\gamma_2(1 - 2\mu)}}{2(1 - 2\mu)}. \end{aligned}$$

The corresponding convergence rate $\rho_o(k)$ is

$$\rho_o(k) = \begin{cases} \rho_{k_1}(k) & \text{if } \mu > \frac{1}{2} \\ \rho_{k_1}(k) & \text{for } \alpha < k < \bar{k} \quad \text{if } \mu < \frac{1}{2}, \\ \rho_{k_2}(k) & \text{for } k > \bar{k} \quad \text{if } \mu < \frac{1}{2} \end{cases}$$

$$\text{where } \rho_{k_1}(k) \stackrel{\text{def}}{=} 1 - \frac{(\alpha - k)^2}{4(k^2\mu + k\gamma_1 + \gamma_2)} \quad \text{and } \rho_{k_2}(k) \stackrel{\text{def}}{=} \mu + \frac{1}{k}(\alpha + \gamma_1) + \frac{\gamma_2}{k^2}.$$

The same quantities can be found as functions of τ :

$$k_o(\tau) \stackrel{\text{def}}{=} \underset{k}{\operatorname{argmin}} z(k, \tau) \quad (27)$$

$$\rho_o(\tau) \stackrel{\text{def}}{=} z(k_o(\tau), \tau). \quad (28)$$

Proposition 13 *With fixed τ , the optimal gain $k_o(\tau)$ is*

given by

$$k_o(\tau) = \begin{cases} \frac{1-\tau\gamma_1}{2\tau\mu} & \text{for } 0 < \tau < \tau_{M_\tau} & \text{if } \mu > \frac{1}{2} \\ \frac{1-\tau\gamma_1}{2\tau\mu} & \text{for } \tau_{m_k} < \tau < \tau_{M_\tau} & \text{if } \mu < \frac{1}{2}, \\ \frac{1}{\tau} & \text{for } 0 < \tau < \tau_{m_k} & \text{if } \mu < \frac{1}{2} \end{cases}$$

where $\tau_{m_k} \stackrel{\text{def}}{=} \frac{1-2\mu}{\gamma_1}$, $\tau_{M_\tau} \stackrel{\text{def}}{=} \min\{\frac{1}{\gamma_1}, \tau_{v_2}^-\}$, and $\tau_{v_2}^- = \frac{-(\gamma_1+\alpha\mu)+\sqrt{(\gamma_1+\alpha\mu)^2+(-\gamma_1^2+4\gamma_2\mu)}}{-\gamma_1^2+4\gamma_2\mu}$. The corresponding convergence rate $\rho_o(\tau)$ is:

$$\rho_o(\tau) = \begin{cases} \rho_{\tau_1}(\tau) & \text{for } 0 < \tau < \tau_{M_\tau} & \text{if } \mu > \frac{1}{2} \\ \rho_{\tau_1}(\tau) & \text{for } \tau_{m_k} < \tau < \tau_{M_\tau} & \text{if } \mu < \frac{1}{2}, \\ \rho_{\tau_2}(\tau) & \text{for } 0 < \tau < \tau_{m_k} & \text{if } \mu < \frac{1}{2} \end{cases}$$

where $\rho_{\tau_1}(\tau) \stackrel{\text{def}}{=} \frac{(-\gamma_1^2+4\gamma_2\mu)\tau^2+2(\gamma_1+2\alpha\mu)\tau+4\mu-1}{4\mu}$ and $\rho_{\tau_2}(\tau) \stackrel{\text{def}}{=} \gamma_2\tau^2 + (\alpha + \gamma_1)\tau + \mu$.

The proofs of Propositions 11–13 are provided in Appendix C.

Figure 5 depicts the quantities defined above: in particular, $\tau(k_o)$ is obtained by inverting $k_o(\tau)$, being this monotonic decreasing, and represents the sampling time for which k_o is the optimal gain. We chose three cases corresponding to $\mu < 1/2$ (Fig. 5a), $1/2 < \mu < 1$ (Fig. 5b), and $\mu > 1$ (Fig. 5c), in order to span the cases given in the previous propositions. Note that $\tau = 1/k$ represents the value s.t. $z^-(k, \tau) = z^+(k, \tau)$. Figure 6 represents the convergence rate ρ_o as a function of k (top plot) and τ (bottom plot). The convergence rate is always smaller than one, hence $\|\mathbf{e}(hT + \tau)\| \leq \|\mathbf{e}(hT)\|$, $\tau \in [0, T]$.

Remark 14 (Sampling time and stabilizability)

Proposition 5 shows that there exists a maximum sampling time T_{\max} s.t. no feedback gain k can ensure stability if $T > T_{\max}$. Conversely, Proposition 11 implies that there exists a threshold τ_{CR} , which can be analytically found by setting $\frac{d\tau_{s1}(k)}{dk} = 0$, s.t. a stabilizing gain always exists if $T < \tau_{CR}$ (see Fig. 1). Such values may help to evaluate the communication hardware to be used.

Control Strategy	$\mathbf{u}_k(hT)$	$\mathbf{u}_{\text{ff}}(hT + \tau)$
SIKM-D (Eq. (14))	$-k_{\text{off}}\mathbf{A}_{\mathbf{q}_h}(\mathbf{q}_h - \mathbf{q}_h^r)$	$\mathbf{A}_{\mathbf{q}_{hT+\tau}}^r \dot{\mathbf{q}}_{hT+\tau}^r$
PS (Eq. (10))	$-k_{\text{on}}\mathbf{A}_{\mathbf{q}_h}(\mathbf{q}_h - \mathbf{q}_h^r)$	$\mathbf{0}$
FF (Eq. (11))	$-k_{\text{on}}\mathbf{A}_{\mathbf{q}_h}(\mathbf{q}_h - \mathbf{q}_h^r)$	$\mathbf{A}_{\mathbf{q}_{hT}} \dot{\mathbf{q}}_{hT+\tau}^r$
SIKM-C (Eq. (12))	$-k_{\text{on}}\mathbf{A}_{\mathbf{q}_h}(\mathbf{q}_h - \mathbf{q}_h^r)$	$\mathbf{A}_{\mathbf{q}_{hT+\tau}}^r \dot{\mathbf{q}}_{hT+\tau}^r$

Table 1

Description of the four strategies used in simulation.

6 Simulation Results

In this section, we implement and compare four techniques for trajectory tracking, which are summarized in Table 1. The first one, named SIKM-D, is the distributed controller (14) proposed in this work, where the gain $k = k_{\text{off}}$ is computed offline following the procedure in Section 5. The last three, referred to as PS, FF, and SIKM-C, respectively, are inspired by the online control strategy proposed in [24] and reported in Appendix D. In particular, they all adopt a centralized communication architecture and differ only in the feedforward term design. Specifically, at the h -th step, k_{on} is the solution to the following optimization problem with initial condition $\mathbf{e}_h = \mathbf{e}(hT)$,

$$\begin{aligned} k_{\text{on}}(hT) &= \underset{k}{\operatorname{argmin}} \|\mathbf{e}(hT + T)\| \\ \text{s. t.} \quad \mathbf{u}(\tau) &= \mathbf{u}_k(hT) + \mathbf{u}_{\text{ff}}(hT + \tau), \end{aligned} \quad (29)$$

where $\tau \in [hT, hT + T]$. The PS technique corresponds to a simple point-stabilization with no feedforward correction, therefore it is expected to always lag behind the desired trajectory. The FF technique implements the naive controller (11) obtained by discretizing the standard continuous-time feedforward term which evaluates the Jacobian at \mathbf{q}_{hT} , that was shown insufficient for asymptotic tracking. Even this strategy is expected to perform worse than SIKM-D despite the potential benefit coming from the online design of the feedback gain. Finally, SIKM-C has the same control structure as SIKM-D, but it re-computes the optimal feedback gain k_{on} at each sampling time. This strategy should provide the best possible performance as opposed to SIKM-D, which computes its gain offline solving a worst-case min-max problem as shown in Section 5. However, SIKM-C requires solving an optimization problem and receiving the state of all robots at each sampling time.

Remark 15 (Distributed vs. centralized control)

In contrast with the centralized scheme, a distributed communication control architecture avoids limitations due to all-to-all wireless communication, such as larger latency or packet loss, and is more robust, cheaper and easier to maintain since it does not depend on the number of robots. Specifically, the distributed communication controller requires only one broadcast communication packet from the load/pivot to the robots, while the centralized communication requires in addition to the broadcast packet also the (possibly synchronized) transmission of N packets from robots to load.

We tested the four techniques on the *Fly-Crane* system [26], whose simulated environment is depicted in Fig. 7. The dynamical model of the system has been developed in a physics-based simulator (*Gazebo*), simulating cables dynamics as well. Simulations have been performed with *software in the loop*, including measurement noise

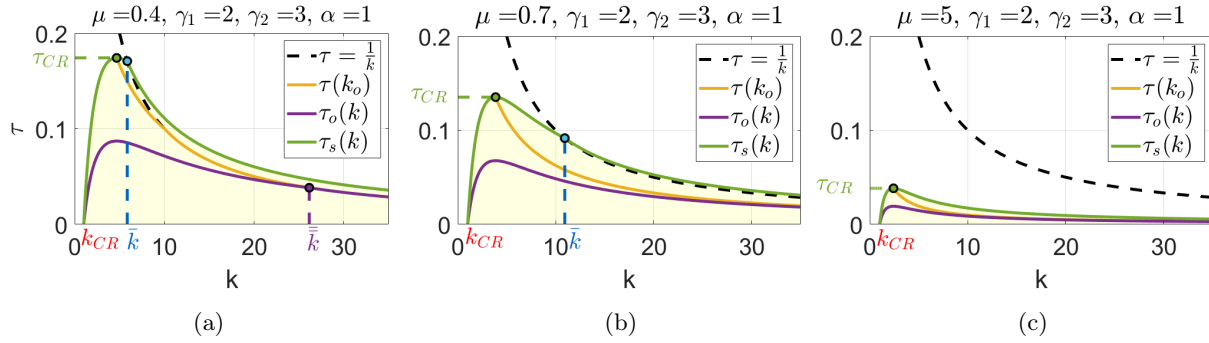


Fig. 5. Representation of the quantities $\tau_s(k)$, $\tau_o(k)$, $\tau(k_0)$ defined in Propositions 11–13.

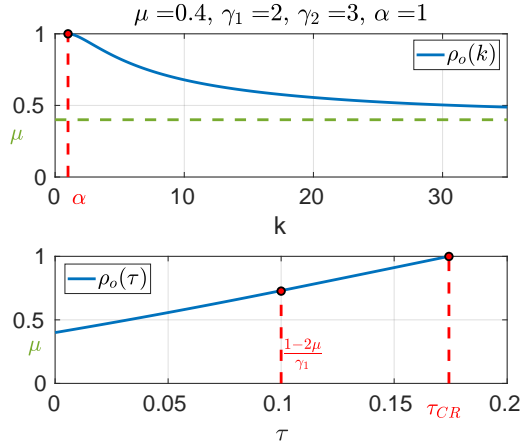


Fig. 6. Estimated convergence rate ρ_0 as a function of the gain k and of the sampling time τ .

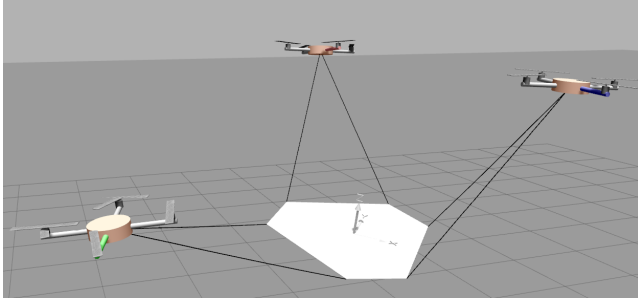


Fig. 7. The Fly-Crane system in the Gazebo simulator.

and communication latency. Communication across the system, planning, and sensing are implemented using the middle-ware *Pocolibs* and the software framework *genoM*, enabling realistic simulations. The simulator of *Fly-Crane* has been used as preliminary validation step for several experiments, such as the ones in [13, 26], proving excellent adherence to the real testbed. Technical details about the simulation software and realistic numerical experiments can be found in [21].

The used system architecture is represented in Fig. 8: a global planner generates offline the desired trajectory

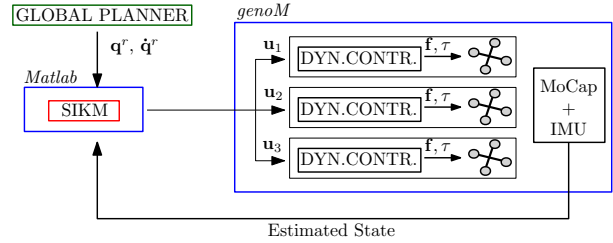


Fig. 8. Architecture used to perform simulations: a global planner generates the desired trajectory $\mathbf{q}^r, \dot{\mathbf{q}}^r$ and sends it to the local planner which generates the desired robot velocities. The blue rectangle on the right represents a realistic environment where the robotic system is simulated.

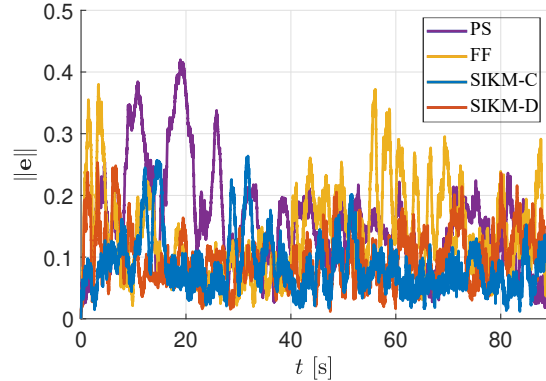


Fig. 9. Tracking error norm $\|\mathbf{e}(t)\| = \|\mathbf{q}(t) - \mathbf{q}^r(t)\|$ obtained with the tracking strategies described in Table 1 ($T = 1.5[s]$).

($\mathbf{q}^r, \dot{\mathbf{q}}^r$) and this information is made available to the SIKM controller, implemented in Matlab-Simulink. The latter generates the desired robot velocities \mathbf{u}_i which are sent to the robots every T seconds via wireless. Then, the low-level dynamical controller (geometric position controller [14]) of each robot converts these velocities into thrust and torque for the quadrotors. An unscented Kalman filter, running at 1 [kHz], fuses the Motion Capture (MoCap) system measurements (at 120 [Hz]) with the IMU measurements (at 1 [kHz]). The estimated system state is then sent to the SIKM controller.

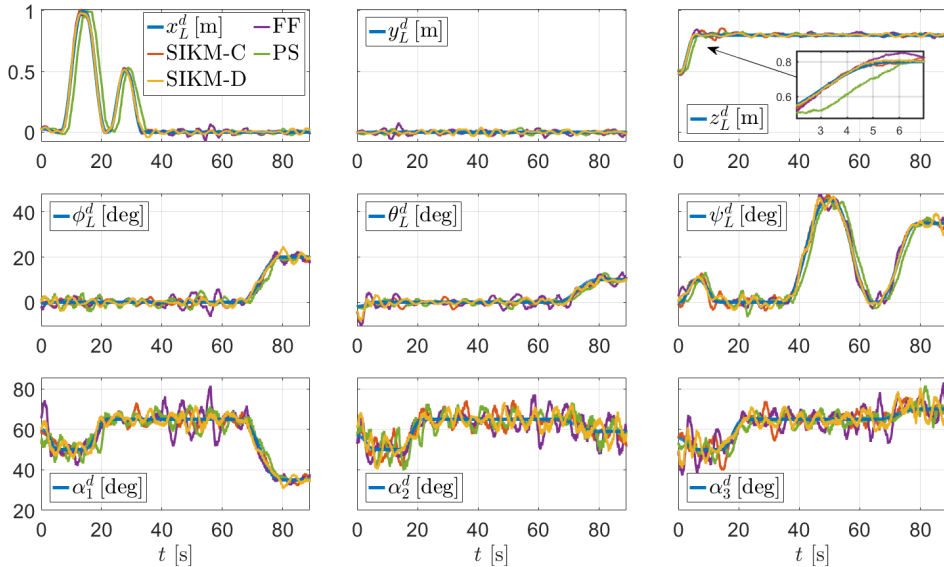


Fig. 10. Comparison of the variables $\mathbf{q}(t)$ in four different simulations, where the tracking strategies described in Table 1 are used. The sampling time is $T = 1.5$ [s]. The first two rows represent respectively the position x_L, y_L, z_L and orientation ϕ_L, θ_L, ψ_L (roll, pitch and yaw) of the load. On the bottom, row the angles $\alpha_i \stackrel{\text{def}}{=} q_i, i = 1, 2, 3$ between cables and load are depicted.

We first compare the tracking error norm for the four control strategies when $T = 1.5$ [s] (see Figs. 9–10). Note that the tracking error does not converge to zero because of non-idealities implemented in simulation, such as sensor noise. The desired trajectory was generated in order to stress all components of \mathbf{q} , except for y -translation because of the system symmetry. From Fig. 10, one can see the benefits of the feedforward term w.r.t. to point-stabilization (PS), which is slower in tracking the desired trajectory as emphasized in the zoom plot of the component z_L . This is because the desired velocity \mathbf{u} is updated only when a new measurement arrives. As for the three feedback-feedforward techniques, SIKM-C and SIKM-D exhibit the best performance. This is highlighted in the zoomed plot of z_L , where FF causes an overshoot.

More interesting and general is the comparison of the four strategies with different sampling times. To compute the feedback gain k_{off} used in the SIKM-D, we first estimated the parameters $[\mu, \alpha, \gamma_1, \gamma_2] = [0.02, 0.13, 0.1, 0.2]$ along the desired trajectory depicted in Fig. 10 for different couples of (k, T) as described in Section 5.1, obtaining the stability region depicted in Fig. 11. Then, for each value of T , we chose the gain k which ensures the highest convergence rate while keeping the system stable, by choosing the x coordinate corresponding to T on the curve $\tau(k_o)$ in Fig. 11. Table 2 reports the observed mean tracking error norms for each strategy. The resulting feedback gain–sampling time pairs (k_{off}, T) were $(2, 0.5)$, $(1.28, 0.75)$ and $(0.67, 1.5)$. Point-stabilization PS yields the largest error which increases quickly with the sampling time. All feedback-feedforward strategies are comparable for short values of T , while SIKM-C and SIKM-D yield

Sampling time T [s]	Mean tracking error norm			
	SIKM-D	SIKM-C	FF	PS
0.5	0.06	0.05	0.05	0.07
0.75	0.06	0.07	0.06	0.10
1.5	0.10	0.09	0.15	0.16

Table 2
Mean tracking error norms obtained in simulation.

the lowest errors for large T . However, we stress that *SIKM-D is distributed*. Hence, the results shown in Table 2 shall be intended in an even stronger way: our proposed distributed controller not only outperforms centralized implementations of standard techniques (point-stabilization and naive feedforward), but is even comparable with its centralized version with online gain adaptation.

To further validate our method under realistic conditions, we also performed simulations with high position measurement noise, comparable to a GPS-based positioning system. As expected, the tracking error remains bounded, proving our design robust. Results of such additional simulations are provided in Appendix E.

7 Conclusions and Future Work

In this paper, we proposed a decentralized controller for multi-robot systems where feedback measurements are transmitted via wireless. We showed that computing the feedforward term is nontrivial, and proposed a strategy to compute the feedback gain with provable stability

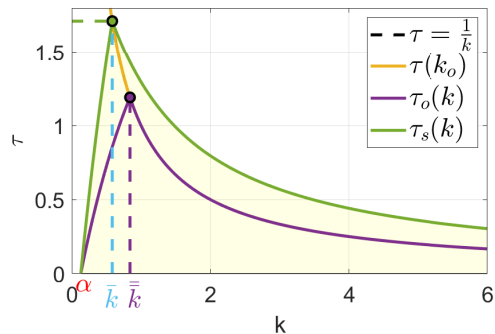


Fig. 11. Stability region, optimal gain k_o , and sampling time τ_o obtained by estimating the parameters μ , α , γ_1 , γ_2 along the trajectory depicted in Fig. 10 for different couples (k, T) .

and convergence guarantees. The more multi-robot systems will become popular and employed for real application, the more sampled-based control strategies will be needed. In this sense, this work paves the way to future developments and practical implementations.

A natural evolution of this work is the implementation of experiments on a real system. Furthermore, an analysis including packets loss and latency, which are typical issues of wireless communication, should be developed.

References

- [1] G. Antonelli and S. Chiaverini. Kinematic control of platoons of autonomous vehicles. *IEEE Trans. Robot.*, 22(6):1285–1292, 2006.
- [2] T. Arai, E. Pagello, L. E. Parker, et al. Advances in multi-robot systems. *IEEE Trans. Robot. Autom.*, 18(5):655–661, 2002.
- [3] R. Conti, E. Meli, A. Ridolfi, and B. Allotta. An innovative decentralized strategy for i-auvs cooperative manipulation tasks. *Robot. Autom. Syst.*, 72:261–276, 2015.
- [4] J. Cortés and M. Egerstedt. Coordinated control of multi-robot systems: A survey. *SICE JCMSI*, 10(6):495–503, 2017.
- [5] D. V. Dimarogonas and K. J. Kyriakopoulos. Distributed cooperative control and collision avoidance for multiple kinematic agents. In *IEEE Conf. Decis. Control*, pages 721–726. IEEE, 2006.
- [6] S. Erhart and S. Hirche. Internal force analysis and load distribution for cooperative multi-robot manipulation. *IEEE Trans. Robot.*, 31(5):1238–1243, 2015.
- [7] H. Farivarnejad and S. Berman. Stability and convergence analysis of a decentralized proportional-integral control strategy for collective transport. In *American Control Conf.*, pages 2794–2801. IEEE, 2018.
- [8] A. Franchi and P. R. Giordano. Online leader selection for improved collective tracking and formation maintenance. *IEEE Control Netw. Syst.*, 5(1):3–13, 2018.
- [9] A. Franchi, C. Masone, V. Grabe, M. Ryll, H. H. Bühlhoff, and P. Robuffo Giordano. Modeling and control of uav bearing formations with bilateral high-level steering. *The Int. J. of Robot. Research*, 31(12):1504–1525, 2012.
- [10] A. Franchi, A. Petitti, and A. Rizzo. Distributed estimation of state and parameters in multi-agent cooperative load manipulation. *IEEE Control Netw. Syst.*, 6(2):690–701, 2019.
- [11] C. Gabellieri, M. Tognon, D. Sanalitra, L. Palottino, and A. Franchi. A study on force-based collaboration in swarms. *Swarm Intelligence*, 14:57–82, 2020.
- [12] T. Hayakawat, T. Matsuzawat, and S. Harat. Formation control of multi-agent systems with sampled information. In *IEEE Conf. Decis. Control*, pages 4333–4338, 2006.
- [13] A. Jiménez-Cano, D. Sanalitra, M. Tognon, A. Franchi, and J. Cortés. Precise cable-suspended pick-and-place with an aerial multi-robot system. *J. Intell. Robot. Syst.*, 105(3):1–13, 2022.
- [14] T. Lee, M. Leoky, and N. H. McClamroch. Geometric tracking control of a quadrotor UAV on SE(3). In *IEEE Conf. Decis. Control*, pages 5420–5425, Atlanta, GA, Dec. 2010.
- [15] Z. Liu, W. Chen, J. Lu, H. Wang, and J. Wang. Formation control of mobile robots using distributed controller with sampled-data and communication delays. *IEEE Trans. Control Syst. Technol.*, 24(6):2125–2132, 2016.
- [16] M. Manubens, D. Devaurs, L. Ros, and J. Cortés. Motion planning for 6-D manipulation with aerial towed-cable systems. In *Robot.: Sci. Syst.*, Berlin, Germany, May 2013.
- [17] C. Masone, H. H. Bühlhoff, and P. Stegagno. Cooperative transportation of a payload using quadrotors: A reconfigurable cable-driven parallel robot. In *IEEE/RSJ Int. Conf. Intell. Robots Syst.*, pages 1623–1630, Oct 2016.
- [18] I. Maza, K. Kondak, M. Bernard, and A. Ollero. Multi-UAV cooperation and control for load transportation and deployment. *J. Intell. Robot. Syst.*, 57(1-4):417–449, 2010.
- [19] D. Mellinger, M. Shomin, N. Michael, and V. Kumar. Cooperative grasping and transport using multiple quadrotors. In *Distr. Auton. Robot. Syst.*, pages 545–558. Springer, 2013.
- [20] G. A. Pereira, M. F. Campos, and V. Kumar. Decentralized algorithms for multi-robot manipulation via caging. *Int. J. Rob. Res.*, 23(7-8):783–795, 2004.
- [21] A. Petitti, D. Sanalitra, M. Tognon, A. Milella, J. Cortés, and A. Franchi. Inertial estimation and energy-efficient control of a cable-suspended load with a team of uavs. In *Int. Conf. Unmanned Aircraft Syst.*, pages 158–165, 2020.
- [22] Y. Ren, S. Sosnowski, and S. Hirche. Fully distributed cooperation for networked uncertain mobile manipulators. *IEEE Trans. Robot.*, 36(4):984–1003, 2020.
- [23] E. Rossi, M. Tognon, R. Carli, A. Franchi, and L. Schenato. Control of over-redundant cooperative manipulation via sampled communication. *arXiv e-prints*, page arXiv:2112.01107, Dec. 2021.
- [24] E. Rossi, M. Tognon, R. Carli, L. Schenato, J. Cortés, and A. Franchi. Cooperative aerial load transportation via sampled communication. *IEEE Contr. Syst. Lett.*, 4(2):277–282, 2020.
- [25] L. Sabattini, C. Secchi, N. Chopra, and A. Gasparri. Distributed control of multirobot systems with global connectivity maintenance. *IEEE Trans. Robot.*, 29(5):1326–1332, 2013.
- [26] D. Sanalitra, H. J. Savino, M. Tognon, J. Cortés, and A. Franchi. Full-pose manipulation control of a cable-suspended load with multiple uavs under uncertainties. *IEEE Robot. Autom. Lett.*, 5:2185–2191, January 2020.
- [27] M. Schwager, B. J. Julian, M. Angermann, and D. Rus. Eyes in the sky: Decentralized control for the deployment of robotic camera networks. *Proc. IEEE*, 99(9):1541–1561, 2011.
- [28] B. Siciliano, L. Sciacicco, L. Villani, and G. Oriolo. *Robotics: Modelling, Planning and Control*. Springer, 2009.

- [29] D. Sieber and S. Hirche. Human-guided multirobot cooperative manipulation. *IEEE Trans. Control Syst. Technol.*, 27(4):1492–1509, 2019.
- [30] E. Simetti and G. Casalino. Manipulation and transportation with cooperative underwater vehicle manipulator systems. *IEEE J. Ocean. Eng.*, 42(4):782–799, 2016.
- [31] K. Sreenath and V. Kumar. Dynamics, control and planning for cooperative manipulation of payloads suspended by cables from multiple quadrotor robots. In *Robot.: Sci. Syst.*, Berlin, Germany, June 2013.
- [32] S. Stramigioli, C. Secchi, A. J. van der Schaft, and C. Fantuzzi. Sampled data systems passivity and discrete port-hamiltonian systems. *IEEE Trans. Robot.*, 21(4):574–587, 2005.
- [33] A. Tagliabue, M. Kamel, R. Siegwart, and J. Nieto. Robust collaborative object transportation using multiple mavs. *Int. J. Rob. Res.*, 38(9):1020–1044, 2019.
- [34] M. Tognon, C. Gabellieri, L. Pallottino, and A. Franchi. Aerial co-manipulation with cables: The role of internal force for equilibria, stability, and passivity. *IEEE Robot. Autom. Lett.*, *Spec. Issue Aerial Manip.*, 3(3):2577 – 2583, 2018.
- [35] A. Tsiamis, C. K. Verginis, C. P. Bechlioulis, and K. J. Kyriakopoulos. Cooperative manipulation exploiting only implicit communication. In *IEEE/RSJ Int. Conf. Intell. Robots Syst.*, pages 864–869. IEEE, 2015.
- [36] C. K. Verginis, A. Nikou, and D. V. Dimarogonas. Communication-based decentralized cooperative object transportation using nonlinear model predictive control. In *European Control Conf.*, pages 733–738. IEEE, 2018.
- [37] Z. Wang and M. Schwager. Force-amplifying n-robot transport system (force-ants) for cooperative planar manipulation without communication. *Int. J. Rob. Res.*, 35(13):1564–1586, 2016.

A Useful Lemmas

Lemma A.1 *Given $\mathbf{x} \in \mathcal{X}$, where $\mathcal{X} \subset \mathbb{R}^n$ is a compact set and given a continuously differentiable function $\mathbf{f}(\mathbf{x}) : \mathbb{R}^n \rightarrow \mathbb{R}^m$ s.t. $\mathbf{f}(\mathbf{0}) = \mathbf{0}$, then there exists $\alpha > 0$ s.t.:*

$$\|\mathbf{f}(\mathbf{x})\| \leq \alpha \|\mathbf{x}\| \quad \forall \mathbf{x} \in \mathcal{X}.$$

PROOF. Since $\mathbf{f}(\mathbf{x})$ is a continuously differentiable function on a compact set, then it is Lipschitz continuous and it holds

$$\mathbf{f}(\mathbf{x}_1 - \mathbf{x}_2) \leq \alpha \|\mathbf{x}_1 - \mathbf{x}_2\|,$$

for some $\alpha > 0$. Now let us call $\mathbf{x} := \mathbf{x}_1$ and $\mathbf{x}_2 = \mathbf{0}$ and we obtain the result of the Lemma.

Lemma A.2 *Given $\mathbf{x} \in \mathcal{X}$ and $\mathbf{y} \in \mathcal{Y}$, where $\mathcal{X} \subset \mathbb{R}^n$, $\mathcal{Y} \subset \mathbb{R}^p$ are compact sets and given a function that is continuously differentiable on the second argument $\mathbf{f}(\mathbf{x}, \mathbf{y}) : \mathbb{R}^n \times \mathbb{R}^p \rightarrow \mathbb{R}^m$ s.t. $\mathbf{f}(\mathbf{x}, \mathbf{0}) = \mathbf{0} \forall \mathbf{x} \in \mathcal{X}$, then there exists $\alpha > 0$ s.t.:*

$$\|\mathbf{f}(\mathbf{x}, \mathbf{y})\| \leq \alpha \|\mathbf{y}\| \quad \forall (\mathbf{x}, \mathbf{y}) \in \mathcal{X} \times \mathcal{Y}.$$

PROOF. The proof is similar to the one of Lemma A.1: being the function continuously differentiable in the second argument, we apply that reasoning on \mathbf{y} :

$$\|\mathbf{f}(\mathbf{x}, \mathbf{y}_1 - \mathbf{y}_2)\| \leq \alpha \|\mathbf{y}_1 - \mathbf{y}_2\|,$$

for some $\alpha > 0$. Now let us call $\mathbf{y} := \mathbf{y}_1$ and $\mathbf{y}_2 = \mathbf{0}$ and we obtain the result of the Lemma.

Lemma A.3 *Given $\mathbf{x} \in \mathcal{X}$, where $\mathcal{X} \subset \mathbb{R}^n$ is a compact set and given two continuously differentiable functions $\mathbf{f}(\mathbf{x}) : \mathbb{R}^n \rightarrow \mathbb{R}^m$, $\mathbf{g}(\mathbf{x}) : \mathbb{R}^n \rightarrow \mathbb{R}^m$ s.t. $\mathbf{f}(\mathbf{0}) = \mathbf{g}(\mathbf{0}) = \mathbf{0}$, then there exists $\alpha > 0$ s.t.:*

$$\|\mathbf{f}(\mathbf{x}) \cdot \mathbf{g}(\mathbf{x})\| \leq \alpha \|\mathbf{x}\|^2 \quad \forall \mathbf{x} \in \mathcal{X}.$$

PROOF. The proof is similar to the one of Lemma A.1. Since both the functions are continuously differentiable on a compact set, then they are also Lipschitz and there exist $a, b > 0$ s.t.

$$\|\mathbf{f}(\mathbf{x})\| \leq a \|\mathbf{x}\|, \quad \|\mathbf{g}(\mathbf{x})\| \leq b \|\mathbf{x}\|,$$

hence

$$\|\mathbf{f}(\mathbf{x}) \cdot \mathbf{g}(\mathbf{x})\| \leq \|\mathbf{f}(\mathbf{x})\| \cdot \|\mathbf{g}(\mathbf{x})\| \leq \alpha \|\mathbf{x}\|^2,$$

where $\alpha := ab > 0$ and we obtain the result of the lemma.

B Error Bound for Point-Stabilization Control

In [24], the authors discussed how, given a desired constant configuration \mathbf{q}^r , if $\mathbf{q}(0) \in \mathcal{B}_d(\mathbf{q}^r)$, the gain k can be designed offline s.t. \mathbf{u}_k in (9) drives the system state to \mathbf{q}^r exponentially fast.

To perform trajectory tracking, the same idea is replicated by assigning a sequence of points as a time-varying reference to the system. In particular, the reference trajectory $\mathbf{q}^r(t)$ is sampled with period T , and the sample points of the sequence $(\mathbf{q}^r(hT), \dot{\mathbf{q}}^r(hT))$ are given as reference configurations one after the other, obtaining controller (10). Such a strategy is indeed commonly used in robotic applications in virtue of its simplicity.

When k is assigned offline, the tracking error is characterized as follows.

Proposition 16 *Consider system (1)–(3) with $\mathbf{u}(t)$ given by (10). There exist $0 < \rho < 1$ and k^* such that, if $\mathbf{q}(0) \in \mathcal{B}_d(\mathbf{q}^r(0))$, $\|\mathbf{q}^r((h+1)T) - \mathbf{q}^r(hT)\| \leq \beta$ for all h with $0 < \beta < (1-\rho)d$, and $0 < k < k^*$, then the tracking error $\mathbf{e}(hT) \stackrel{\text{def}}{=} \mathbf{q}(hT) - \mathbf{q}^r(hT)$ is bounded, i.e.,*

$$\|\mathbf{e}(hT)\| \leq \rho d + \frac{\beta}{1-\rho}, \quad \forall h \in \mathbb{N},$$

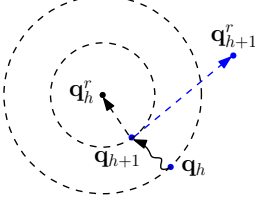


Fig. B.1. Trajectory tracking by using the point stabilization strategy.

and in particular

$$\lim_{h \rightarrow +\infty} \|\mathbf{e}(hT)\| \leq \frac{\beta}{1 - \rho}.$$

PROOF. As shown in Fig. B.1, at time $t = hT$ the system state is $\mathbf{q}_h = \mathbf{q}(hT)$ and the reference point is \mathbf{q}_h^r ; then, at time $t = (h + 1)T$, the new system state is $\mathbf{q}_{h+1} = \mathbf{q}((h+1)T)$ and a new reference \mathbf{q}_{h+1}^r is assigned. This strategy is applied every T seconds. In [24, Proposition 6] the authors showed that, given a configuration \mathbf{q}_h and the desired one \mathbf{q}_h^r , there exists a feedback gain s. t.

$$\|\mathbf{e}((h + 1)T)\| \leq \rho_h \|\mathbf{e}(hT)\|, \quad (\text{B.1})$$

where $\rho_h \in (0, 1)$ is defined in [24, Proposition 5] and depends on the set $\mathcal{B}_d(\mathbf{q}^r(hT))$. In virtue of Assumption 1.i), we consider $\rho = \max_h \rho_h$ as an upper bound for the convergence rate over all the trajectory samples. Equation (B.1) implies that the error decreases by at least a factor ρ between two consecutive sampling times. Further, it is shown in [24] that the error also decreases at each time instant $t \in (hT, (h + 1)T)$. Now, we define the quantities

$$\mathbf{e}_{h+1}^+ \stackrel{\text{def}}{=} \mathbf{q}_{h+1} - \mathbf{q}_{h+1}^r, \quad \mathbf{e}_{h+1}^- \stackrel{\text{def}}{=} \mathbf{q}_{h+1} - \mathbf{q}_h^r.$$

In words, \mathbf{e}_{h+1}^- is the error between configuration \mathbf{q}_{h+1} and the desired one \mathbf{q}_h^r , while \mathbf{e}_{h+1}^+ is the error between \mathbf{q}_{h+1} and the next desired configuration \mathbf{q}_{h+1}^r . In view of (B.1) and assumption $\|\mathbf{q}_{h+1}^r - \mathbf{q}_h^r\| \leq \beta$, it holds

$$\begin{aligned} \|\mathbf{e}_{h+1}^-\| &= \|\mathbf{q}_{h+1} - \mathbf{q}_h^r\| \leq \rho \|\mathbf{q}_h - \mathbf{q}_h^r\| = \rho \|\mathbf{e}_h^+\| \\ \|\mathbf{e}_{h+1}^+\| &= \|\mathbf{q}_{h+1} - \mathbf{q}_h^r + \mathbf{q}_h^r - \mathbf{q}_{h+1}^r\| \\ &\leq \|\mathbf{q}_{h+1} - \mathbf{q}_h^r\| + \|\mathbf{q}_h^r - \mathbf{q}_{h+1}^r\| \\ &= \|\mathbf{e}_{h+1}^-\| + \|\mathbf{q}_h^r - \mathbf{q}_{h+1}^r\| \leq \rho \|\mathbf{e}_h^+\| + \beta. \end{aligned}$$

Being $\beta < (1 - \rho)d$, it follows $\|\mathbf{e}_{h+1}^+\| < d$ and therefore Proposition 6 in [24] can be applied s.t. the error decrease (B.1) holds for reference point \mathbf{q}_{h+1}^r in an iterative fashion. Now, we find an upper bound to the steady-

state tracking error: iterating the last inequality, it holds

$$\begin{aligned} \|\mathbf{e}_1^+\| &\leq \rho \|\mathbf{e}_0^+\| + \beta \\ \|\mathbf{e}_2^+\| &\leq \rho \|\mathbf{e}_1^+\| + \beta \leq \rho^2 \|\mathbf{e}_0^+\| + \rho\beta + \beta \\ &\vdots \\ \|\mathbf{e}_h^+\| &\leq \rho^h \|\mathbf{e}_0^+\| + \beta \sum_{i=0}^{h-1} \rho^i = \rho^h \|\mathbf{e}_0^+\| + \beta \frac{1 - \rho^h}{1 - \rho}. \end{aligned}$$

The overall upper bound for the error norm can be deduced in virtue of the assumptions $\|\mathbf{e}_0^+\| < d$ and $\rho < 1$. In particular, at the limit it follows

$$\lim_{h \rightarrow +\infty} \|\mathbf{e}_h^+\| \leq \lim_{h \rightarrow +\infty} \beta \frac{1 - \rho^h}{1 - \rho} = \frac{\beta}{1 - \rho}. \quad \square$$

C Proofs of Propositions 11–13

C.1 Proof of Proposition 11

Recall that the stability time $\tau_s(k)$ is s.t. $z(k, \tau) < 1$ for $k > \alpha, 0 < \tau < \tau_s(k)$. Hence the goal now is to find an expression for $\tau_s(k)$ by studying the inequality

$$z(k, \tau) < 1,$$

From the definition of the function $z(k, \tau)$, we can distinguish three cases: $k\tau < 1$, $k\tau = 1$, $k\tau > 1$.

(1) $k\tau < 1$: In this case

$$z(k, \tau) = z^-(k, \tau) = 1 + \tau(\alpha - k) + \tau^2(k^2\mu + k\gamma_1 + \gamma_2).$$

We are interested to understand when $z^-(k, \tau) < 1$, that is to find the maximum τ for which $\|\mathbf{e}(hT + \tau)\| < \|\mathbf{e}(hT)\|$.

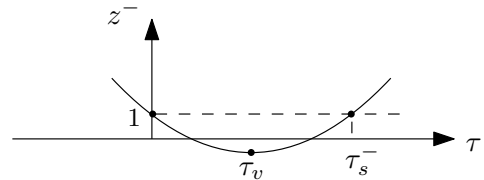


Fig. C.1. Representation of $z(k, \tau)$ in the case $k\tau < 1$ and $k > \alpha$.

$$\begin{aligned} z^-(k, \tau) &< 1 \\ \Leftrightarrow 1 + \tau(\alpha - k) + \tau^2(k^2\mu + k\gamma_1 + \gamma_2) &< 1 \\ \Leftrightarrow p_s^-(k) := \tau(\alpha - k) + \tau^2(k^2\mu + k\gamma_1 + \gamma_2) &< 0. \end{aligned}$$

$p_s^-(k)$ represents an upward parabola with solutions

$$\tau_{s_1}^- = 0, \quad \tau_{s_2}^- = \frac{k - \alpha}{k^2\mu + k\gamma_1 + \gamma_2}.$$

Hence $p_s^-(k) < 0$ if $0 < \tau < \tau_{s_2}^-$; as a consequence $z^-(k, \tau) < 1$ if $0 < \tau < \tau_{s_2}^-$. Let us define

$$\tau_s^- := \tau_{s_2}^-.$$

Now let us check when $\tau_s^- < \frac{1}{k}$, that is

$$\begin{aligned} \frac{k - \alpha}{k^2\mu + k\gamma_1 + \gamma_2} &< \frac{1}{k} \\ \Leftrightarrow p_{s_2}^-(k) &:= k^2(1 - \mu) - k(\alpha + \gamma_1) - \gamma_2 < 0. \end{aligned}$$

The solutions are

$$k_{s_{1,2}}^- = \frac{\alpha + \gamma_1 \pm \sqrt{(\alpha + \gamma_1)^2 + 4\gamma_2(1 - \mu)}}{2(1 - \mu)}.$$

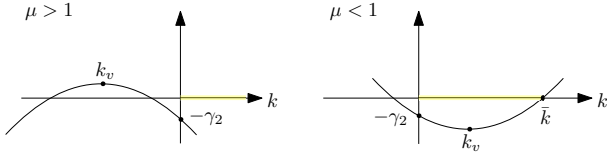


Fig. C.2. Representation of $p_{s_2}^-(k)$.

- if $\mu < 1$, then $p_{s_2}^-(k)$ is an upward parabola such that the solutions and the vertex k_v satisfy

$$\sum \text{sol} = \frac{\alpha + \gamma_1}{1 - \mu} > 0, \quad \prod \text{sol} = \frac{-\gamma_2}{1 - \mu} < 0$$

$$k_v = \frac{\alpha + \gamma_1}{2(1 - \mu)} > 0.$$

Hence, if $\mu < 1$, then $\tau_s^- < \frac{1}{k}$ for $\alpha < k < \bar{k}$, where

$$\begin{aligned} \bar{k} &= \max\{k_{s_1}^-, k_{s_2}^-\} = \\ &\begin{cases} \frac{\alpha + \gamma_1 + \sqrt{(\alpha + \gamma_1)^2 + 4\gamma_2(1 - \mu)}}{2(1 - \mu)} & \text{if } \mu < 1 \\ \frac{\alpha + \gamma_1 - \sqrt{(\alpha + \gamma_1)^2 + 4\gamma_2(1 - \mu)}}{2(1 - \mu)} & \text{if } \mu > 1 \end{cases}. \end{aligned} \quad (\text{C.1})$$

In this case $\mu < 1$, hence $\bar{k} = \frac{\alpha + \gamma_1 + \sqrt{(\alpha + \gamma_1)^2 + 4\gamma_2(1 - \mu)}}{2(1 - \mu)}$.

- if $\mu > 1$, then $p_{s_2}^-(k)$ is a downward parabola such that

$$\sum \text{sol} < 0, \quad \prod \text{sol} > 0$$

$$k_v < 0.$$

Hence, if $\mu > 1$, then $\tau_s^- < \frac{1}{k} \forall k > \alpha$.

In conclusion,

$$z^-(k, \tau) < 1 \text{ if } 0 < \tau < \tau_s^-$$

$$\tau_s^- < \frac{1}{k} \text{ if } \begin{cases} \alpha < k < \bar{k} & \text{if } \mu < 1 \\ k > \alpha & \text{if } \mu > 1 \end{cases}$$

(2) $k\tau = 1$: In this case

$$z\left(k, \frac{1}{k}\right) = \mu + \frac{1}{k}(\alpha + \gamma_1) + \frac{\gamma_2}{k^2}.$$

For which values of k is $z(k, \frac{1}{k}) < 1$?

$$\mu + \frac{1}{k}(\alpha + \gamma_1) + \frac{\gamma_2}{k^2} < 1$$

$$p_s^-(k) := k^2(\mu - 1) + k(\alpha + \gamma_1) + \gamma_2 < 0. \quad (\text{C.2})$$

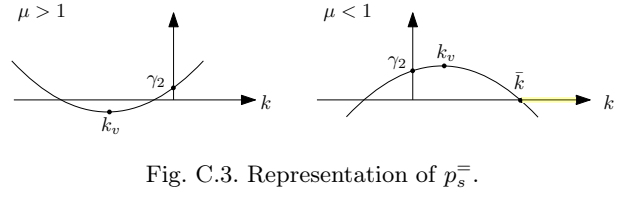


Fig. C.3. Representation of p_s^- .

- $\mu < 1$: p_s^- is a concave downward parabola. In $k = 0$ the parabola intersects the y-axis in $\gamma_2 > 0$. Now the vertex of the parabola is in $k_v^- > 0$, the sum of the solutions is $\sum \text{sol} > 0$ and product $\prod \text{sol} < 0$. Finally, $z(k, \frac{1}{k}) < 1$ where $p_s^-(k) < 0$, that is for $k > \bar{k}$, where $\bar{k} := \max\{k_{s_1}^-, k_{s_2}^-\}$ has the same value that we have found in (C.1).
- $\mu > 1$: p_s^- is a concave upward parabola. In $k = 0$ the parabola intersects the y-axis in $\gamma_2 > 0$. The vertex of the parabola is in

$$k_v^- = \frac{\alpha + \gamma_1}{2(1 - \mu)} < 0.$$

The sum and product of the solutions are

$$\sum \text{sol} = \frac{\alpha + \gamma_1}{1 - \mu} < 0, \quad \prod \text{sol} = \frac{\gamma_2}{\mu - 1} > 0,$$

hence the solutions are both negative and $p_s^-(k)$ is always positive, so $z(k, \frac{1}{k}) > 1 \forall k > \alpha$ if $\mu > 1$.

In conclusion:

$$z(k, 1/k) < 1 \text{ for } \begin{cases} \nexists k > \alpha & \text{if } \mu > 1 \\ k > \bar{k} & \text{if } \mu < 1 \end{cases}.$$

(3) $k\tau > 1$: In this case

$$z(k, \tau) = z^+(k, \tau) = -1 + \tau(\alpha + k) + \tau^2(k^2\gamma_1 + k\gamma_2 + \gamma_3).$$

This is an upward parabola with vertex

$$\tau_v^+ = -\frac{k + \alpha}{2(k^2\gamma_1 + k\gamma_2 + \gamma_3)} < 0$$

Notice that $z^+(k, 0) = -1 < 0$ and

$$\begin{aligned} \sum \text{sol} &= -\frac{\alpha + k}{k^2\mu + k\gamma_1 + \gamma_2} < 0 \\ \prod \text{sol} &= -\frac{1}{k^2\mu + k\gamma_1 + \gamma_2} < 0. \end{aligned}$$

For which values of k is $z^+(k, \tau) < 1$?

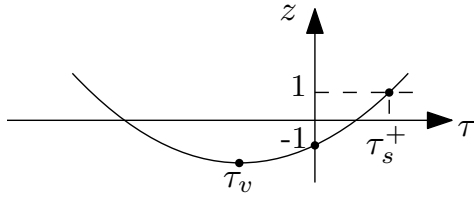


Fig. C.4. Representation of $z(k, \tau)$ in the case $k\tau > 1$.

$$z^+(k, \tau) < 1$$

$$\Leftrightarrow -1 + \tau(\alpha + k) + \tau^2(k^2\mu + k\gamma_1 + \gamma_2) < 1$$

$$\Leftrightarrow p_s^+(k) := \tau^2(k^2\mu + k\gamma_1 + \gamma_2) + \tau(\alpha + k) - 2 < 0.$$

$p_s^+(k)$ represents an upward parabola with solutions s.t.

$$\begin{aligned} \sum \text{sol} &= -\frac{\alpha + k}{k^2\mu + k\gamma_1 + \gamma_2} < 0 \\ \prod \text{sol} &= -\frac{2}{k^2\mu + k\gamma_1 + \gamma_2} < 0 \end{aligned}$$

$$\tau_{s_1}^+ = \frac{-(\alpha + k) - \sqrt{(\alpha + k)^2 + 8(k^2\mu + k\gamma_1 + \gamma_2)}}{2(k^2\mu + k\gamma_1 + \gamma_2)}$$

$$\tau_{s_2}^+ = \frac{-(\alpha + k) + \sqrt{(\alpha + k)^2 + 8(k^2\mu + k\gamma_1 + \gamma_2)}}{2(k^2\mu + k\gamma_1 + \gamma_2)}$$

We define

$$\tau_s^+ := \max\{\tau_{s_{1,2}}^+\} = \tau_{s_2}^+$$

and $z^+(k, \tau) < 1$ for $0 < \tau < \tau_s^+$. Notice that in this case we have to check for which k it holds $\tau_s^+ > \frac{1}{k}$

since we are analyzing the case $k\tau > 1$:

$$\begin{aligned} \tau_s^+ &> \frac{1}{k} \\ \frac{-(\alpha + k) + \sqrt{(\alpha + k)^2 + 8(k^2\mu + k\gamma_1 + \gamma_2)}}{2(k^2\mu + k\gamma_1 + \gamma_2)} &> \frac{1}{k} \\ -k(\alpha + k) + k\sqrt{(\alpha + k)^2 + 8(k^2\mu + k\gamma_1 + \gamma_2)} &> \\ &> 2(k^2\mu + k\gamma_1 + \gamma_2) \\ k^2((\alpha + k)^2 + 8(k^2\mu + k\gamma_1 + \gamma_2)) &> k^2(\alpha + k)^2 + \\ &+ 4(k^2\mu + k\gamma_1 + \gamma_2)^2 + 4k(\alpha + k)(k^2\mu + k\gamma_1 + \gamma_2) \\ 8k^2(k^2\mu + k\gamma_1 + \gamma_2) &> 4(k^2\mu + k\gamma_1 + \gamma_2)^2 + \\ &+ 4k(\alpha + k)(k^2\mu + k\gamma_1 + \gamma_2) \\ 2k^2 &> (k^2\mu + k\gamma_1 + \gamma_2) + k(\alpha + k) \\ k^2(1 - \mu) - k(\alpha + \gamma_1) - \gamma_2 &> 0 \\ p_{\tau_s^+}(k) &:= k^2(\mu - 1) + k(\alpha + \gamma_1) + \gamma_2 < 0 \end{aligned}$$

The solutions are

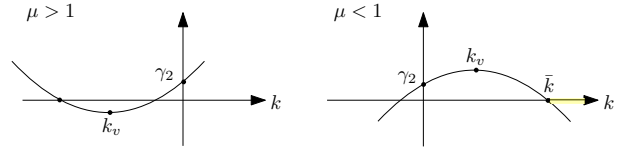


Fig. C.5. Representation of $p_{\tau_s^+}(k)$.

$$k_{\pm} = \frac{\alpha + \gamma_1 \pm \sqrt{(\alpha + \gamma_1)^2 + 4\gamma_2(1 - \mu)}}{2(1 - \mu)}$$

- $\mu > 1$: $p_{\tau_s^+}(k)$ is an upward parabola s.t. for $k = 0$ it intersects the y-axis in γ_2 and

$$\sum \text{sol} = -\frac{\alpha + \gamma_1}{\mu - 1} < 0, \quad \prod \text{sol} = \frac{\gamma_2}{\mu - 1} < 0$$

As a consequence, this parabola is never negative for $k > 0$, hence $\tau_s^+ < \frac{1}{k} \forall k > 0$.

- $\mu < 1$: $p_{\tau_s^+}(k)$ is a downward parabola and

$$\sum \text{sol} > 0, \quad \prod \text{sol} > 0$$

As a consequence, it is negative for $k > \bar{k}$, hence $\tau_s^+ > \frac{1}{k}$ for $k > \bar{k} = \max\{k_{\pm}\}$, that is the same value found in (C.1).

In conclusion,

$$z^+(k, \tau) < 1 \text{ if } 0 < \tau < \tau_s^+$$

$$\tau_s^+ \begin{cases} < \frac{1}{k} \text{ for } k > \alpha & \text{if } \mu > 1 \\ > \frac{1}{k} \text{ for } k > \bar{k} & \text{if } \mu < 1 \end{cases}$$

Notice that only if $\mu < 1$, then τ_s^+ belongs to the region $k\tau > 1$ that we are considering. Otherwise, we have to consider τ_s^- instead.

Hence $\tau_s = \tau_s^-$ if $\mu > 1$ or if $\mu < 1$ and $\alpha < k < \bar{k}$, whereas $\tau_s = \tau_s^+$ if $\mu < 1$ and $k > \bar{k}$, that is

$$\begin{aligned} \tau_s(k; \mu, \gamma_1, \gamma_2) &= \frac{k - \alpha}{k^2\mu + k\gamma_1 + \gamma_2} \text{ if } \mu > 1 \\ \tau_s(k; \mu, \gamma_1, \gamma_2) &= \begin{cases} \frac{k - \alpha}{k^2\mu + k\gamma_1 + \gamma_2} & \text{for } \alpha < k < \bar{k} \\ \frac{-(\alpha + k) + \sqrt{(\alpha + k)^2 + 8(k^2\mu + k\gamma_1 + \gamma_2)}}{2(k^2\mu + k\gamma_1 + \gamma_2)} & \text{for } k > \bar{k} \end{cases} \text{ if } \mu < 1 \end{aligned}$$

C.2 Proof of Proposition 12

Recall that the optimal time $\tau_o(k)$ is s.t. $z(k, \tau_o(k))$ reaches its minimum value. Hence the goal now is to find an expression for $\tau_o(k)$.

From the definition of the function $z(k, \tau)$, we can distinguish two cases: $k\tau < 1$, $k\tau > 1$.

(1) $k\tau < 1$: In this case

$$z(k, \tau) = z^-(k, \tau) = 1 + \tau(\alpha - k) + \tau^2(k^2\mu + k\gamma_1 + \gamma_2)$$

$z(k, \tau)$ is an upward parabola (see Fig. C.1) with vertex at

$$\tau_v^- = \frac{k - \alpha}{2(k^2\mu + k\gamma_1 + \gamma_2)} \quad (\text{C.3})$$

Notice that $\tau_v^- > 0$ since $k > \alpha$. The value of the function at the vertex corresponds to its minimum:

$$\begin{aligned} z(k, \tau_v) &= 1 - \frac{(k - \alpha)^2}{2(k^2\mu + k\gamma_1 + \gamma_2)} + \\ &+ \frac{(k - \alpha)^2}{4(k^2\mu + k\gamma_1 + \gamma_2)^2} (k^2\mu + k\gamma_1 + \gamma_2) = \\ &= 1 - \frac{1}{4} \frac{(k - \alpha)^2}{(k^2\mu + k\gamma_1 + \gamma_2)} < 1 \end{aligned}$$

Now we want to check if $\tau_v^- < \frac{1}{k}$, that is if the minimum value belongs to the region we are analyzing:

$$\begin{aligned} \tau_v^- &= \frac{k - \alpha}{2(k^2\mu + k\gamma_1 + \gamma_2)} < \frac{1}{k} \\ \Leftrightarrow k^2 - k\alpha &< 2\mu k^2 + 2\gamma_1 k + 2\gamma_2 \\ \Leftrightarrow p_v^-(k) &:= k^2(1 - 2\mu) - k(\alpha + 2\gamma_1) - 2\gamma_2 < 0 \end{aligned} \quad (\text{C.4})$$

where the solutions of $p_v^-(k)$

$$k_{\pm} = \frac{\alpha + 2\gamma_1 \pm \sqrt{(\alpha + 2\gamma_1)^2 + 8\gamma_2(1 - 2\mu)}}{2(1 - 2\mu)}$$

are s.t.

$$\sum \text{sol} = \frac{\alpha + 2\gamma_1}{1 - 2\mu}, \quad \prod \text{sol} = \frac{-2\gamma_2}{1 - 2\mu}$$

where there exist two different solutions if $(\alpha + 2\gamma_1)^2 + 8\gamma_2(1 - 2\mu) > 0$, that is

$$\mu < \frac{(\alpha + 2\gamma_1)^2}{16\gamma_2} + \frac{1}{2}$$

otherwise τ_v^- is always greater than $1/k$.

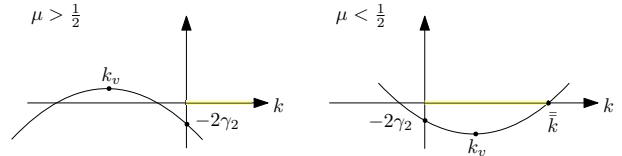


Fig. C.6. Representation of $p_v^-(k)$.

- if $1 - 2\mu > 0$, that is $\mu < \frac{1}{2}$, then $p_v^-(k)$ is an upward parabola with solutions k_{\pm} s.t. $\sum \text{sol} > 0$, $\prod \text{sol} < 0$ and $\tau_v < \frac{1}{k}$ if $\alpha < k < \bar{k}$, where

$$\begin{aligned} \bar{k} &:= \max\{k_-, k_+\} = \\ &= \begin{cases} \frac{\alpha + 2\gamma_1 + \sqrt{(\alpha + 2\gamma_1)^2 + 8\gamma_2(1 - 2\mu)}}{2(1 - 2\mu)} & \text{if } \mu < \frac{1}{2} \\ \frac{\alpha + 2\gamma_1 + \sqrt{(\alpha + 2\gamma_1)^2 + 8\gamma_2(1 - 2\mu)}}{2(1 - 2\mu)} & \text{if } \mu > \frac{1}{2} \end{cases} \end{aligned} \quad (\text{C.5})$$

- if $1 - 2\mu < 0$, that is $\mu > \frac{1}{2}$, then $p_v^-(k)$ is a downward parabola with solutions k_{\pm} s.t. $\sum \text{sol} < 0$, $\prod \text{sol} > 0$ and $\tau_v < \frac{1}{k}$ if $k > \alpha$.

In conclusion,

$$\tau_v^- < \frac{1}{k} \text{ if } \begin{cases} \alpha < k < \bar{k} & \text{if } \mu < \frac{1}{2} \\ k > \alpha & \text{if } \mu > \frac{1}{2} \end{cases}$$

So τ_v^- represents the optimal time in the case $k\tau < 1$ for $\alpha < k < \bar{k}$ if $\mu < \frac{1}{2}$ and for $k > \alpha$ if $\mu > \frac{1}{2}$.

(2) $k\tau > 1$. In this case

$$z(k, \tau) = z^+(k, \tau) = -1 + \tau(\alpha + k) + \tau^2(k^2\gamma_1 + k\gamma_2 + \gamma_3)$$

we still have an upward parabola with vertex

$$\tau_v^+ = -\frac{k + \alpha}{2(k^2\gamma_1 + k\gamma_2 + \gamma_3)} < 0$$

Since $\tau_v^+ < 0$ it cannot be a valid optimal time and, since $z(k, \tau)$ is a monotonically increasing function in k and τ , then the minimum can be detected in $\tau = 1/k$.

Finally $\tau_o(k) = \tau_v^-(k)$ for $\alpha < k < \bar{k}$ if $\mu < \frac{1}{2}$ and for $k > \alpha$ if $\mu > \frac{1}{2}$, whereas $\tau_o(k) = 1/k$ for $k > \bar{k}$ if $\mu < \frac{1}{2}$, that is

$$\tau_o(k; \mu, \gamma_1, \gamma_2) = \frac{k - \alpha}{2(k^2\mu + k\gamma_1 + \gamma_2)} \text{ if } \mu > \frac{1}{2}$$

$$\tau_o(k; \mu, \gamma_1, \gamma_2) = \begin{cases} \frac{k - \alpha}{2(k^2\mu + k\gamma_1 + \gamma_2)} & \text{for } \alpha < k < \bar{k} \\ \frac{1}{k} & \text{for } k > \bar{k} \end{cases} \text{ if } \mu < \frac{1}{2}$$

Computation of the convergence rate

The convergence rate, defined in (26), corresponds to the function $z(k, \tau)$ evaluated in $\tau = \tau_o(k)$:

$$\rho(k) = z(k, \tau_o)$$

We have already seen that, depending on the value of the parameter μ , then $\tau_o(k)$ has different values and $z(k, \tau_o(k))$ too:

- $0 < \mu < \frac{1}{2}$:

$$\tau_o = \begin{cases} \tau_v^- & \text{if } \alpha < k < \bar{k} \\ \frac{1}{k} & \text{if } k > \bar{k} \end{cases}$$

and

$$\rho(k) = z^-(k, \tau_o) = \begin{cases} z^-(k, \tau_v^-) = 1 - \frac{(\alpha - k)^2}{4(k^2\mu + k\gamma_1 + \gamma_2)} & \text{if } \alpha < k < \bar{k} \\ z(k, \frac{1}{k}) = \mu + \frac{1}{k}(\alpha + \gamma_1) + \frac{1}{k^2}\gamma_2 & \text{if } k > \bar{k} \end{cases}$$

Notice that $z^-(k, \tau_o) < 1$ always and $z(k, \frac{1}{k}) < 1$ in the case it is considered ($\mu < \frac{1}{2}$). Moreover, note that for $\gamma_1 = \gamma_2 = 0$, $z^-(k, \frac{1}{k}) = \mu + \frac{\alpha}{k}$ that tends to μ for large values of k :

$$\rho(k) \rightarrow \begin{cases} 1 - \frac{1}{4\mu} & \text{if } \alpha < k < \bar{k} \\ \mu & \text{if } k > \bar{k} \end{cases}$$

- $\mu > \frac{1}{2}$: in this case

$$\rho = z^-(k, \tau_v^-) = 1 - \frac{(\alpha - k)^2}{4(k^2\mu + k\gamma_1 + \gamma_2)} \quad \forall k > \alpha$$

and for $\gamma_1 = \gamma_2 = 0$ and big values of k :

$$\rho(k) \rightarrow 1 - \frac{1}{4\mu} \quad \forall k > \alpha$$

C.3 Proof of Proposition 13

- (1) $k\tau < 1$:

Let us rewrite the function $z^-(k, \tau)$ s.t. it depends on k , since τ is assumed to be fixed now.

$$z^-(k, \tau) = \tau^2\mu k^2 + \tau(\tau\gamma_1 - 1)k + 1 + \tau\alpha + \tau^2\gamma_2 \quad (\text{C.6})$$

The function represents an upward parabola with vertex

$$k_v^- = \frac{1 - \tau\gamma_1}{2\tau\mu} > 0 \text{ if } \tau < \frac{1}{\gamma_1}$$

Let us check when $k_v^- < \frac{1}{\tau}$:

$$\frac{1 - \tau\gamma_1}{2\tau\mu} < \frac{1}{\tau} \quad \Leftrightarrow \quad \tau > \frac{1 - 2\mu}{\gamma_1}$$

Observe that if $\mu > \frac{1}{2}$, then $\frac{1 - 2\mu}{\gamma_1} < 0$, hence $\tau > \frac{1 - 2\mu}{\gamma_1}$ always and $k_v^- < \frac{1}{\tau}$.

In conclusion,

$$k_v^- < \frac{1}{\tau} \text{ if } \tau > \frac{1 - 2\mu}{\gamma_1}$$

Now we find out when $z^-(k_v^-, \tau) < 1$. First of all we compute the expression $z^-(k_v^-, \tau)$:

$$\begin{aligned} z^-(k_v^-, \tau) &= \tau^2\mu \frac{(1 - \tau\gamma_1)^2}{4\tau^2\mu^2} + \tau(\tau\gamma_1 - 1) \frac{1 - \tau\gamma_1}{2\tau\mu} + \tau^2\gamma_2 + \\ &+ \tau\alpha + 1 = \\ &= \frac{(1 - \tau\gamma_1)^2}{4\mu} - \frac{(1 - \tau\gamma_1)^2}{2\mu} + \tau^2\gamma_2 + \tau\alpha + 1 \\ &= -\frac{(1 - \tau\gamma_1)^2}{4\mu} + \tau^2\gamma_2 + \tau\alpha + 1 \\ &= \frac{(-\gamma_1^2 + 4\gamma_2\mu)\tau^2 + 2(\gamma_1 + 2\alpha\mu)\tau + 4\mu - 1}{4\mu} \end{aligned}$$

Now, under which conditions does it hold $z^-(k_v^-, \tau) < 1$?

$$\begin{aligned} \frac{(-\gamma_1^2 + 4\gamma_2\mu)\tau^2 + 2(\gamma_1 + 2\alpha\mu)\tau + 4\mu - 1}{4\mu} &< 1 \\ \Leftrightarrow (-\gamma_1^2 + 4\gamma_2\mu)\tau^2 + 2(\gamma_1 + 2\alpha\mu)\tau + 4\mu - 1 &< 4\mu \\ p_v^-(\tau) := (-\gamma_1^2 + 4\gamma_2\mu)\tau^2 + 2(\gamma_1 + 2\alpha\mu)\tau - 1 &< 0 \end{aligned} \quad (\text{C.7})$$

$p_v^-(\tau)$ is a parabola in τ with vertex in

$$\tau_v^- = -\frac{\gamma_1 + 2\alpha\mu}{-\gamma_1^2 + 4\gamma_2\mu} > 0 \quad \text{if } \mu < \frac{\gamma_1^2}{4\gamma_2}$$

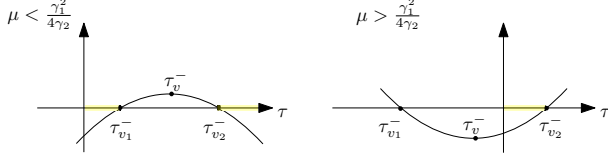


Fig. C.7. Representation of $p_v^-(\tau)$.

The solutions of (C.7) are

$$\tau_{v1}^- = \frac{-(\gamma_1 + \alpha\mu) - \sqrt{(\gamma_1 + \alpha\mu)^2 + (-\gamma_1^2 + 4\gamma_2\mu)}}{-\gamma_1^2 + 4\gamma_2\mu}$$

$$\tau_{v2}^- = \frac{-(\gamma_1 + \alpha\mu) + \sqrt{(\gamma_1 + \alpha\mu)^2 + (-\gamma_1^2 + 4\gamma_2\mu)}}{-\gamma_1^2 + 4\gamma_2\mu}$$

Notice that

$$\sum \text{sol} = \frac{\gamma_1 + \alpha\mu}{\gamma_1^2 - 4\gamma_2\mu} > 0 \quad \text{if} \quad \mu < \frac{\gamma_1^2}{4\gamma_2}$$

$$\prod \text{sol} = \frac{1}{\gamma_1^2 - 4\gamma_2\mu} > 0 \quad \text{if} \quad \mu < \frac{\gamma_1^2}{4\gamma_2}$$

Moreover the argument of the square root is always positive and $\tau_{v1}^- < \tau_{v2}^-$ if $\mu > \frac{\gamma_1^2}{4\gamma_2}$.

Finally, the concavity of $p_v^-(\tau)$ is upward if $\mu > \frac{\gamma_1^2}{4\gamma_2}$, otherwise it is downward. You can see these results in Fig. C.7.

In conclusion, $z^-(k_v^-, \tau)$:

$$\begin{cases} < 1 \text{ for } 0 < \tau < \tau_{v2}^- \vee \tau > \tau_{v1}^- & \text{if } \mu < \frac{\gamma_1^2}{4\gamma_2} \\ < 1 \text{ for } 0 < \tau < \tau_{v2}^- & \text{if } \mu > \frac{\gamma_1^2}{4\gamma_2} \end{cases}$$

(2) $k\tau = 1$

Even if the stability analysis has been performed in the scenario where k was fixed, we will analyze the stability on the curve $k = \frac{1}{\tau}$ because the result will be useful when we will compute the convergence rate.

$$z\left(\frac{1}{\tau}, \tau\right) = \gamma_2\tau^2 + (\alpha + \gamma_1)\tau + \mu$$

Let us check when $z\left(\frac{1}{\tau}, \tau\right) < 1$:

$$\gamma_2\tau^2 + (\alpha + \gamma_1)\tau + \mu < 1$$

$$\Leftrightarrow p^-(\tau) := \gamma_2\tau^2 + (\alpha + \gamma_1)\tau + \mu - 1 < 0$$

$p^-(\tau)$ is an upward parabola with vertex

$$\tau_v^- = \frac{-(\alpha + \gamma_1)}{2\gamma_2} < 0$$

and solutions

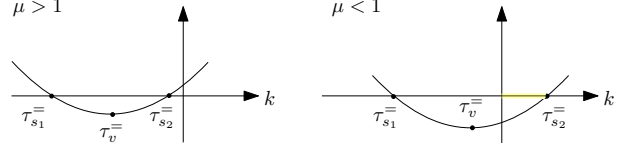


Fig. C.8. Representation of $p_s^-(k, \tau)$.

$$\tau_{s1,2}^- = \frac{-(\alpha + \gamma_1) \pm \sqrt{(\alpha + \gamma_1)^2 - 4\gamma_2(\mu - 1)}}{2\gamma_2}$$

s.t.

$$\sum \text{sol} = -\frac{\alpha + \gamma_1}{\gamma_2} < 0$$

$$\prod \text{sol} = \frac{\mu - 1}{\gamma_2} > 0 \quad \text{if} \quad \mu > 1$$

In conclusion:

$$z\left(\frac{1}{\tau}, \tau\right) < 1 \text{ for } \begin{cases} \nexists \tau > 0 & \text{if } \mu > 1 \\ 0 < \tau < \tau_{s2}^- & \text{if } \mu < 1 \end{cases}$$

(3) $k\tau > 1$:

Let us rewrite the function $z^+(k, \tau)$ s.t. it depends on k , since τ is assumed to be fixed now.

$$z^+(k, \tau) = \tau^2\mu k^2 + \tau(\tau\gamma_1 + 1)k + \tau^2\gamma_2 k + \tau\alpha - 1 \quad (\text{C.8})$$

The function represents an upward parabola with vertex

$$k_v^+ = -\frac{1 + \tau\gamma_1}{2\tau\mu} < 0 \text{ for } \tau > 0$$

Hence k_v^+ never belongs to the region $k\tau > 1$.

In conclusion $k_o(\tau) = k_v^-$ for $0 < \tau < \frac{1}{\gamma_1}$ if $\mu > \frac{1}{2}$ and for $\frac{1-2\mu}{\gamma_1} < \tau < \frac{1}{\gamma_1}$ if $\mu < \frac{1}{2}$; instead, $k_o(\tau) = \frac{1}{\tau}$ for $0 < \tau < \frac{1-2\mu}{\gamma_1}$ if $\mu < \frac{1}{2}$, that is

$$k_o(\tau; \mu, \gamma_1, \gamma_2) = \frac{1 - \tau\gamma_1}{2\tau\mu} \text{ for } \tau < \frac{1}{\gamma_1} \text{ if } \mu > \frac{1}{2}$$

$$k_o(\tau; \mu, \gamma_1, \gamma_2) = \begin{cases} \frac{1 - \tau\gamma_1}{2\tau\mu} & \text{for } \frac{1-2\mu}{\gamma_1} < \tau < \frac{1}{\gamma_1} \\ \frac{1}{\tau} & \text{for } 0 < \tau < \frac{1-2\mu}{\gamma_1} \end{cases} \text{ if } \mu < \frac{1}{2}$$

Computation of the convergence rate

The convergence rate, defined in (28), corresponds to the function $z(k, \tau)$ evaluated in $\tau = \tau_o(k)$:

$$\rho(\tau) = z(k_o, \tau)$$

We have already seen that, depending on the value of the parameter μ , then $k_o(\tau)$ has different values and $z(k_o(\tau), \tau)$ too:

- $0 < \mu < \frac{1}{2}$:

$$k_o = \begin{cases} k_v^- & \text{for } \frac{1-2\mu}{\gamma_1} < \tau < \frac{1}{\gamma_1} \\ \frac{1}{\tau} & \text{for } 0 < \tau < \frac{1-2\mu}{\gamma_1} \end{cases}$$

and

$$\begin{aligned} \rho(\tau) &= z^-(k_o, \tau) = \\ &= \begin{cases} z^-(k_v^-, \tau) & \text{for } \frac{1-2\mu}{\gamma_1} < \tau < \frac{1}{\gamma_1} \\ z(\frac{1}{\tau}, \tau) & \text{for } 0 < \tau < \frac{1-2\mu}{\gamma_1} \end{cases} \\ &= \begin{cases} \frac{(-\gamma_1^2 + 4\gamma_2\mu)\tau^2 + 2(\gamma_1 + 2\alpha\mu)\tau + 4\mu - 1}{4\mu} & \text{for } \frac{1-2\mu}{\gamma_1} < \tau < \frac{1}{\gamma_1} \\ \gamma_2\tau^2 + (\alpha + \gamma_1)\tau + \mu & \text{for } 0 < \tau < \frac{1-2\mu}{\gamma_1} \end{cases} \end{aligned}$$

- $\mu > \frac{1}{2}$: in this case

$$\begin{aligned} \rho(\tau) &= z^-(k_v^-, \tau) = \\ &= \frac{(-\gamma_1^2 + 4\gamma_2\mu)\tau^2 + 2(\gamma_1 + 2\alpha\mu)\tau + 4\mu - 1}{4\mu} \\ &\text{for } 0 < \tau < \frac{1}{\gamma_1} \end{aligned}$$

D Online Gain Design Proposed in [24]

Let us introduce the following auxiliary system,

$$\begin{aligned} \dot{\mathbf{q}}'(\tau; \mathbf{q}_h) &= -\mathbf{A}_{\mathbf{q}'(\tau; \mathbf{q}_h)}^{-1} \mathbf{A}_{\mathbf{q}_h} \mathbf{q}_h =: \mathbf{f}(\mathbf{q}'(\tau); \mathbf{q}_h) \quad (\text{D.1}) \\ \mathbf{q}'(0; \mathbf{q}_h) &= \mathbf{q}_h; \quad \mathbf{q}_h \in \mathcal{B}_d(\mathbf{q}^r), \end{aligned}$$

with $\mathbf{q}_h \stackrel{\text{def}}{=} \mathbf{q}(hT)$. Being $\mathbf{f}(\mathbf{q}; \mathbf{q}) = -\mathbf{q}$, it holds $\|\mathbf{q}'(0^+; \mathbf{q}_h) - \mathbf{q}^r\| < \|\mathbf{q}_h - \mathbf{q}^r\|$. Also, we define

$$\tau_s(\mathbf{q}_h) \stackrel{\text{def}}{=} \min_{\tau} \{\tau < 0 \mid \|\mathbf{q}'(\tau; \mathbf{q}_h)\| = \|\mathbf{q}_h\|\}, \quad (\text{D.2})$$

$$\tau_o(\mathbf{q}_h) \stackrel{\text{def}}{=} \operatorname{arginf}_{0 \leq \tau \leq \tau_s(\mathbf{q}_h)} \|\mathbf{q}'(\tau; \mathbf{q}_h)\|, \quad (\text{D.3})$$

where $\tau_s(\mathbf{q}_h) = \infty$ if $\|\mathbf{q}'(\tau; \mathbf{q}_h) - \mathbf{q}^r\| < \|\mathbf{q}_h - \mathbf{q}^r\|, \forall \tau$. Then, k_h is designed as (see [24, Proposition 7])

$$k_h = \frac{\tau_o(\mathbf{q}_h)}{T}. \quad (\text{D.4})$$

E Additional Simulations

In Fig. E.1, we show the behavior of the system state when increasing the noise variance of the sensor that collects data from the MoCap system. $\sigma_2 = 0.003$ is the variance used for the previous simulations, while $\sigma_1 = 0.01$ is the one used for this simulation. You can notice that, as expected, the performance become worse when

increasing the noise variance and the oscillations around the reference trajectory become bigger. This result shows that our strategy can handle uncertain measurements of the state \mathbf{q} while guaranteeing stability of the system.

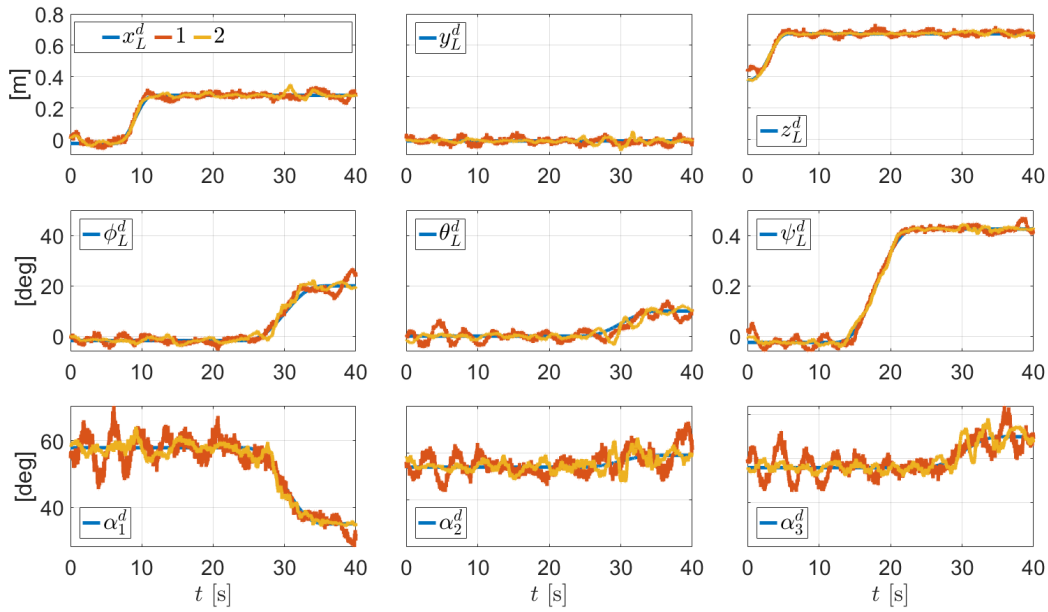


Fig. E.1. Comparison of the variables $\mathbf{q}(t)$ for two different values $\sigma_1 = 0.01$ and $\sigma_2 = 0.003$ of noise variance of the sensor vision (the values 1 and 2 in the legend refer to $\sigma_{1,2}$): the tracking strategy SIKM-D is implemented with sampling time $T = 0.75$ [s] and feedback gain $k_{\text{off}} = 1.28$. The first two rows represent respectively the position x_L, y_L, z_L and orientation ϕ_L, θ_L, ψ_L (roll, pitch and yaw) of the load. On the last row the angles $\alpha_i \stackrel{\text{def}}{=} q_i, i = 1, 2, 3$ between the cables and the load are depicted. Notice that the oscillations around the reference trajectory become bigger as the noise variance increases.